EXPERIMENTAL STUDY OF CONCENTRIC SHORT HELICAL ANTENNAS

David E. Gates

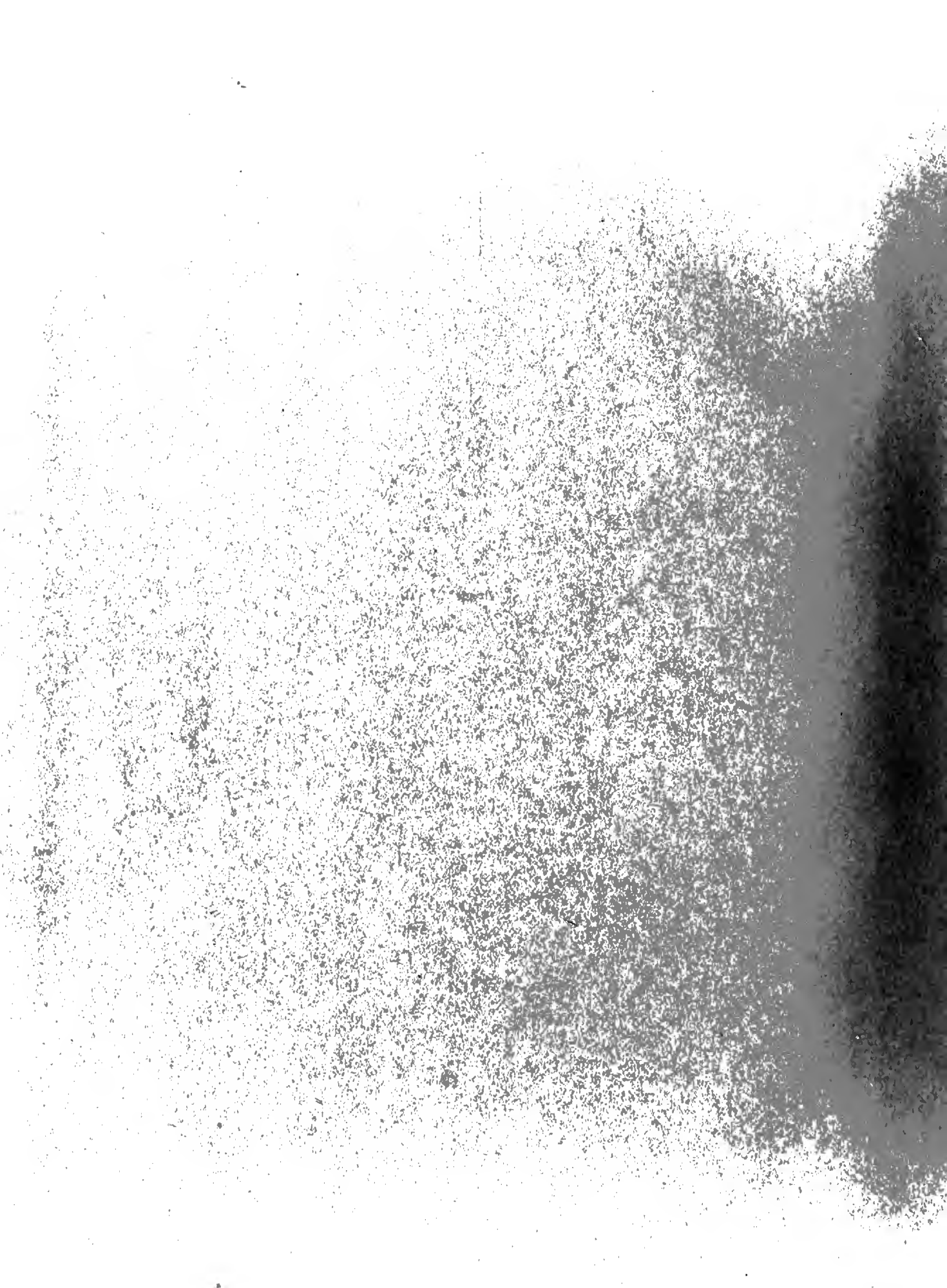

26

EXPERIMENTAL STUDY OF CONCENTRIC SHORT HELICAL ANTENNAS

* * * * *

David E. Gates

EXPERIMENTAL STUDY OF

CONCENTRIC SHORT HELICAL ANTENNAS

by

David E. Gates

Lieutenant, United States Navy

Submitted in partial fulfillment of
the requirements for the degree of

MASTER OF SCIENCE
IN
ENGINEERING ELECTRONICS

United States Naval Postgraduate School
Monterey, California

1 9 5 7

EXPERIMENTAL STUDY OF

CONCENTRIC SHORT HELICAL ANTENNAS

by

David E. Gates

This work is accepted as fulfilling
the thesis requirements for the degree of

MASTER OF SCIENCE

IN

ENGINEERING ELECTRONICS

from the

United States Naval Postgraduate School

ABSTRACT

Modern airborne electronic counter-measures systems require broad-band antenna configurations. The concentric nesting of helices covering adjacent frequency bands would reduce the bulk of an helical antenna configuration to satisfy the needs of such a system.

An array of one-and-a-quarter-turn helices is developed, which will give axial ratios of less than three to one and beamwidths greater than 30^{o} over a 2.5 to one bandwidth.

A model explaining the behavior of tilt is developed and is applied to the helical array.

I wish to thank Mr. William Scharfman and Dr. Tetsu Morita of the Stanford Research Institute for their aid and advice in the preparation of this study.

TABLE OF CONTENTS

Section	Title	Page
1.	Introduction	1
2.	The Helix	3
3.	Coordinates	6
4.	Scaling	7
5.	Investigation Procedure	8
6.	Representation of Results	11
7.	The Concentric Array	13
8.	Results of Measurements	
	A. The Three-Turn Helical Antenna	14
	B. The Three-Turn Scaled Array	15
	C. Unbalanced Scaled Array	17
	D. 1 1/4-Turn Scaled Array	18
	E. Equal-Spacing Array	19
	F. Helices in a Cavity	20
	G. Top-Loading Effects	21
	H. Cross-Wound Helices	22
9.	Tilt	23
10.	Summary	27
11.	Bibliography	55

LIST OF ILLUSTRATIONS

Figure		Page
1.	Helix Parameters	29
2.	The Coordinate System	30
3.	Simplified Block Diagram of the Pattern Range	30
4.	Power Radiation Pattern using Rotating Polarization	31
5.	Measured Radiation Pattern Characteristics of a 13.5°, three-turn Helix	32
6.	Measured Impedance of 13.5°, three-turn Helix	33
7.	Illustrative Optimum-Filter Feed for the Concentric Array	34
8.	Measured Radiation Pattern Characteristics of a 13.5°, three-turn Helix, having a 0.625-scaled parasite	35
9.	Measured Impedance of a 13.5°, three-turn Helix, having a 0.625-scaled parasite	36
10.	Measured Radiation Pattern Characteristics of a 13.5°, three-turn Helix, having a 1.6-scaled parasite	37
11.	Measured Radiation Pattern Characteristics of a 13.5°, three-turn Helix, having a 1.6-scaled 1 7/8-turn parasite	38
12.	Measured Radiation Pattern Characteristics of a 13.5°, 1 1/4-turn Helix, having a 1.6-scaled parasite	39
13.	Measured Radiation Pattern Characteristics of a 13.5°, 1 1/4-turn Array.	40
14.	Measured Radiation Pattern Characteristics of the Equal-Spacing Array	41
15.	Measured Radiation Pattern Characteristics of the Equal-Spacing Array (Slug-loaded)	42
16.	Measured Radiation Pattern Characteristics of the Equal-Spacing Array, $D_1/D_2 = 1.95$	43

Figure		Page
17.	Measured Radiation Pattern Characteristics of the Equal-Spacing Array, $D_1/D_2 = 1.95$ (Slug-loaded)	44
18.	The Cavity Mounting	45
19.	Measured Radiation Pattern Characteristics of a Cavity-Mounted Array	46
20.	Measured Radiation Pattern Characteristics of a Cavity-Mounted Array (Slug-loaded)	47
21.	Measured Impedance of a Cavity-Mounted Array (Slug-loaded)	48
22.	Measured Radiation Pattern Characteristics of a One-turn, Cavity-Mounted Array	49
23.	Measured Radiation Pattern Characteristics of a One-turn, Cavity-Mounted Array (Slug-loaded)	50
24.	Measured Radiation Pattern Characteristics of a Cross-Wound, Cavity-Mounted Array	51
25.	The Even and Odd Radiation Modes	52
26.	Tilt of an Axial Beam Pattern due to Multimoding	53
27.	The Concentric, "Odd-Mode" Array	54

TABLE OF SYMBOLS AND ABBREVIATIONS

a	Unit vector
AR	Axial ratio
b	Radius of a uniline conductor above a ground plane
c	Velocity of free-space electromagnetic propagation
C	Circumference of right circular cylinder passing through helix conductor center
d	Helix conductor diameter
D	Diameter of right circular cylinder passing through helix conductor center
E	Electric field magnitude
f_n	Normalized frequency
F	Scaling factor, or ratio of similar dimensions of two helices of different sizes
h	Height of center of a uniline conductor above the ground plane
h_c	Depth of cavity
H	Magnetic field magnitude
l_s	Length of loading slug
n	Number of turns
R_0	Normal radiation mode
R_1	Axial-beam radiation mode
R_2	Radiation mode where $C \doteq 2\lambda$
S	Spacing, or axial length of one turn
VSWR	Voltage standing-wave ratio
Z_0	Characteristic Impedance
Z_1	Terminal impedance of large antenna when in the non-operating optimum filter condition
Z_2	Terminal impedance of small antenna when in the non-operating optimum filter condition

α Pitch angle

λ Free-space wavelength

θ Angle of spherical coordinate radius vector from axis

ϕ Angle of spherical coordinate radius vector from the ground plane reference

Subscript notation is self-explanatory.

Vector quantities are noted by a $-$ over the magnitude, e.g., $\bar{E}$. Unit vectors are noted by a $\wedge$, e.g., $\hat{a}_\phi$. Absolute values are noted by $| \; |$ around the quantity.

1. Introduction.

Airborne electronic counter-measure systems have long required antenna arrays providing adequate coverage of the frequency spectrum above 60 megacycles per second. The recent concept of "wide-open" receiver detection is designed to receive any frequency occurring within a broad spectrum. Elements, such as tunable antenna loading elements, cannot provide this "wide-open" operation. Thus, the antenna arrays used must be passive. Tuned antennas, such as resonant dipoles are unsuitable due to the number required to give adequate bandwidth. Antennas exhibiting broadband operation are indicated.

The helical antenna exhibits broadband operation which on the surface seems to fit this concept admirably. At frequencies where the circumference of a helix is approximately equal to a wavelength, the helix radiates in the axial mode.[1] In this mode, the radiation pattern is a broad, elliptically polarized lobe along the helix axis. In this frequency region, the phase velocity of the guided wave (along the conductor) varies almost directly with frequency. This self-adjustment of the current distribution maintains the end-fire pattern over almost an octave of bandwidth. The input and radiation impedance over this range varies slowly and may be considered a constant if matching is not critical. This simplifies the matching networks required, allowing transformers or their microwave equivalents to be used. In addition, the elliptic polarization assures the effective reception of signals of all linear polarizations.

[1] J. D. Kraus, Antennas, McGraw-Hill Book Company, Inc., 1950, p. 173.

Unlike most thin-wire antennas, the helix occupies "three-dimensional" volume. This is a serious disadvantage when one considers the thinness of modern airfoil structures necessary for near sonic speeds. Attempts to improve the ratio of the operating bandwidth to the volume are reflected in the examination of tapered helices, short helices, and spiral antennas.[1,2,3,4,5] While these examinations are directed toward single radiating elements, such an improvement might be obtained in certain arrays having two or more elements.

Stanford Research Institute conducted a preliminary investigation of two concentric (coaxial) helical antennas in 1955. This study indicated that such an array might be practical, and would reduce the volume occupied by the array. "Array" is used in the sense of a collection of antennas serving the same system.

This subsequent examination is primarily experimental. First, consideration is given to the radiation pattern of the array. The principal characteristics of this pattern are usable beam widths, degree of elliptical polarization, and axial directivity. No consideration was given to aircraft structure other than a study of the array enclosed in a metal cavity.

[1]J. S. Chatterjee, Radiation Field of a Conical Helix, J. Appl. Phys., 24, pp. 550-559, May 1953.

[2]J. S. Chatterjee, Radiation Characteristics of a Conical Helix of Low Pitch Angle, J. Appl. Phys., 26, pp. 331-335.

[3]P. W. Springer, End Loaded and Expanding Helices as Broad Band Circularly Polarized Radiators, Proc. Natl. Electronics Conf., Vol. 5, pp. 161-171, 1949.

[4]A. Bystrom, Jr. and D. G. Berntsen, An Experimental Investigation of Cavity-Mounted Helical Antennas, I.R.E. Transactions on Antennas and Propagation, AP-4, pp. 53-58, January 1949.

[5]Discussion of the spiral antenna by John Elgin of the Dalmo-Victor Company on 31 July 1956.

2. The Helix.

The helix has long been used as an inductive circuit element where its dimensions are small compared with a free-space wavelength. Its slow-wave properties have found applications in traveling-wave tube design wherein the phase velocity of the axial wave is slowed to provide effective interaction with a high-velocity electron beam.

While the helical inductor has been used to physically shorten resonant dipole antennas, extensive examination of its radiation properties when the physical dimensions are comparable to a wavelength is relatively recent. The circularly polarized normal radiation mode was presented barely a decade ago.[1] Literature concerning the axial mode began appearing at about the same time.[2] Experimental studies of uniform helices were conducted by John D. Kraus and his associates at Ohio State University.[3,4,5,6,7,8,9] Primarily, these studies were confined to

[1]H. A. Wheeler, A Helical Antenna for Circular Polarization, Proc. I.R.E., 35, pp. 1484-1488, December 1947.

[2]J. D. Kraus, Helical Beam Antenna, Electronics, 20, pp. 109-111, April 1947.

[3]J. D. Kraus and J. C. Williamson, Characteristics of Helical Antennas Radiating in the Axial Mode, J. Appl. Phys., 19, pp. 87-96, January 1948.

[4]O. J. Glasser and J. D. Kraus, Measured Impedances of Helical Beam Antennas, J. Appl.Phys., 19, pp. 193-197, February 1948.

[5]J. D. Kraus, Helical Beam Antennas for Wide-band Applications, Proc. I.R.E., 36, pp. 1236-1242, October 1948.

[6]J. D. Kraus, The Helical Antenna, Proc. I.R.E., 37, pp. 263-272, March 1949.

[7]J. D. Kraus, Helical Beam Antenna Design Techniques, Communications, 29, pp. 6-9, pp. 34-35, September 1949.

[8]T. E. Tice and J. D. Kraus, The Influence of Conductor Size on the Properties of Helical Beam Antennas, Proc. I.R.E., 37, p. 1296, November 1949.

[9]J. D. Kraus, Antennas, McGraw-Hill Book Company, Inc., 1950.

This latter text is a comprehensive compilation of references 2 to 8 and will be the only one footnoted in the remainder of this paper.

helices of greater than three turns, although alternate configurations are indicated. The proposed array is one of those.[1]

When its circumference is approximately one free-space wavelength the helix radiates in the axial or beam (R_1) mode. This mode results in an end-fire, well-defined radiated beam. The axial field is usually elliptically polarized. The normal frequency range of this mode is about 1.6 to one, extending from a helix circumference of .83 wavelengths to a circumference of about 1.3 wavelengths.[2]

For a uniform helix of three turns or greater, the impedance, axial ratio, and radiation beam characteristics remain relatively constant over the R_1 frequency range, wherein the helix parameters (see Figure 1) do not markedly affect the resulting pattern. Pitch angles (α) may vary from 8° to 20°. Wire diameters (d) may be chosen from $.006\lambda$ to $.05\lambda$. The regularity of the radiation pattern is established if the number of turns is greater than three, but the beamwidth varies inversely as the square root of the number of turns. Antennas having pitch angles from 12° to 14° give optimum axial ratios and directivity.[3]

Experimental radiation patterns for long ($n > 3$) helices agree closely with patterns derived mathematically assuming the current distribution along the helix conductor to be a sinusoidal forward-traveling wave.[4] Current distribution measurements show that the actual current distribution may be more closely approximated by the sum of four distributions,

[1] J. D. Kraus, op. cit., p. 214

[2] J. D. Kraus, op. cit., pp. 178, 193.

[3] J. D. Kraus, op. cit., pp. 208-210.

[4] E. T. Kornhauser, Radiation Field of Helical Angennas with Sinusoidal Current, J. Appl. Phys., 22, pp. 887-891, July 1951.

a constant forward wave, a lesser constant reflected wave, and exponentially attenuated forward and reflected waves. In most cases the exponential decay may be considered complete after a little more than one turn.[1]

Where the helix is short, the radiated energy of the reflected waves is comparable with that of the forward waves and the current distribution may no longer be approximated by a single forward-traveling wave. Capacitive or dissipative top-loading of the helix reduces the reflection coefficient of the open end. This may be accomplished by loops, slugs, lossy dielectric, or other means which effect proper reflection impedances.[2,3] With proper end-loading, the operation of the short helix may be assumed similar to that of the longer, except for an array factor affecting beam width.

The coupling of the helix operating in the axial mode is very low for dielectric structures inside the helix. However, dielectrics and conductors outside the helix cylinder do affect the radiation pattern and the impedance. This coupling decreases with increasing separation and becomes negligible for cavity enclosures when the cavity has a diameter approximately twice that of the helix.[4]

[1]Kraus, op. cit., p. 184.

[2]Springer, loc. cit.

[3]O. C. Haycock and J. S. Ajioka, Radiation Characteristics of Helical Antennas of Few Turns, Proc. I.R.E., 40, pp. 989-991, August 1952.

[4]Bystrom and Berntsen, loc. cit.

3. Coordinates.

A spherical coordinate system is selected such that the array axis coincides with the line, $\theta = 0^{\circ}$. The base termination of the larger helix lies in the plane, $\phi = 270^{\circ}$. This is illustrated in Figure 2. The origin lies in the plane, $\theta = 90^{\circ}$, containing the termination of the helix proper (i.e., above the feed network).

It is convenient to define θ polarization as that component parallel to the unit vector, $\hat{a}_{\theta}$, and to define ϕ polarization as that component parallel to the unit vector, $\hat{a}_{\phi}$.

4. Scaling.

Inasmuch as the helix is capable of scaling, the following descriptions and graphs of results will be expressed in terms of a normalized frequency, f_n. This frequency is chosen such that the corresponding free-space wavelength is equal to the circumference of the larger filamentary helix. Thus,

$$f_n = c/C_1 = c/\pi D_1.$$

All dimensions will be expressed in terms of the diameter of the larger helix, D_1.

5. Investigation Procedure.

This investigation was confined primarily to the radiation patterns of various concentric helical antenna arrays. A simplified block diagram of the pattern range system is shown in Figure 3. The audio-frequency signal generator supplies a modulating sine or square wave to the radio-frequency oscillator. The modulated radio-frequency signal is transmitted through a rotating coaxial joint to a linearly polarized transmitting antenna. A remotely controlled, reversible, electric motor rotates this antenna at a constant speed. This provides continuous rotation of the polarization of the signal, all polarizations having been transmitted in one-half revolution of the antenna. Remote synchro indication allows fixed-positioning of the antenna in polarization by stopping the drive motor when the proper angle is reached.

The array to be measured was mounted on a copper plate about one wavelength in diameter for the lowest frequency used and this was extended by a copper screen ground plane approximately four wavelengths square at the lowest frequency used. The edges of this ground plane were rounded back on an approximate one wavelength radius. The edges of the copper screen were serrated and twisted in a random fashion to prevent resonant edge-current distributions.

The ground plane and array were mounted on a non-metallic tower. The tower is hydraulically driven in rotation in the horizontal plane. A second hydraulic drive rotates the spindle, to which the array is attached, in a vertical plane. The speed of rotation of either system is continuously variable and separate synchro position indications are available to remote indicators and to the polar plotter.

The radio-frequency signal is detected immediately in back of the ground plane by a bolometer detector mounted in a slide tuner. This minimizes radio-frequency attenuation and stray radiation coupling to the antenna circuit. The slide tuner provides impedance matching.

The detected audio signal is returned through shielded cable to a transformer-coupled amplifier. Bolometer current is provided by a battery and resistor in series with the transformer primary. The amplifier incorporates a fixed-element, calibrated attenuator to check the linearity of the amplifier-plotter circuitry. The polar plotter receives a magnitude (pen) input from the amplifier and a rotational (turntable) input from the tower or spindle synchro.

Usually the radiation pattern of an antenna is described by two patterns. The first is a pattern of the radiated field in the plane of ϕ = a constant, with θ polarization, and the second is in the same plane with ϕ polarization. Ellipticity and beamwidth values deduced from these measurements assume axial symmetry of the radiated pattern and, further, assume time quadrature between the fields of the two orientations. These patterns are obtained on the above range, when the tower-rotation is the input to the synchro of the plotter and the transmitting antenna is fixed at the proper polarization.

The range is capable of another type of representation, due to the rotating polarization capabilities of the transmitting antenna. Consider the receiving antenna to be fixed at some angular orientation exhibiting elliptical polarization, while the transmitting antenna is rotated. The received signal will vary with the varying polarization of the transmitted signal. Thus the pen will indicate a maximum, after a 90° rotation of the transmitting antenna, a minimum, and, after an 180° rotation, the

maximum again. It is seen that the maximum and minimum cross-polarized fields are sampled each half revolution of the transmitting antenna. This technique does not require knowledge of the orientation of the polarization of axes of ellipticity.[1] Further, if the tower is rotated slowly with respect to the transmitting antenna, these maximum and minimum samples may be used to construct envelopes of tangency which will be called the major and minor patterns, and will give, at a glance, the ellipticity of the antenna for the particular cross-section. This pattern is illustrated in Figure 4.

This procedure may also be used for conical cuts (θ = a constant), and will give a measure of the circular symmetry of the radiation pattern unobtainable with fixed polarization ranges. It is to be noted, however, that no information regarding the absolute polarization of the resultant fields is contained in this pattern. Such information can be obtained by additional patterns with a known, fixed polarization.

The major and minor patterns represent the major and minor axes of the polarization ellipse and are in time quadrature.

Repeatability of both major and minor patterns is good. While the rotation of the transmitting antenna is not synchronized with model rotation, pattern envelopes can be reproduced with an error of less than five per cent.

Frequency increments were restricted to one-sixth of an octave or less. It is felt that this is sufficient to illustrate the behavior of the helical array over its frequency range.

[1]The axes of ellipticity are usually, but not always, found to be parallel to $\hat{a}_\phi$ and $\hat{a}_\theta$.

6. Representation of Results.

While a compilation of the polar power plots gives a very complete representation of the behavior of the radiation pattern of the antenna array, the information is not in a readily available form for comparison or application studies. Plots showing the variation with frequency of beamwidth, ellipticity, and impedance provide a reasonable measure of a beam pattern's desirability.

In the process of reduction of data, it was found that the short helix exhibited tendencies toward tilt that were not capable of simple graphical representation. Tilt is the off-axis location of the maximum field of either the major or the minor radiation pattern. In Figure 4, it is noticed that both of these patterns are tilted to the left, with the maxima occurring at about $\theta = 10^{o}$. At certain frequencies, patterns were found where the tilts of the major and minor patterns occurred at differing angular orientations of the model.

This characteristic of the short helix made attempts to rigidly define beamwidth unsuitable, since tilt was usually accompanied by assymmetry of the radiation patterns. In considering the airborne application of the radiators, a degree of significance must be attached to the desirability of having beamwidth centered about the axis. Therefore, beamwidth is arbitrarily plotted as either the angle between the half power points (symmetrical beams) of the minor pattern, or as twice the angle from the helix axis to the nearest direction exhibiting half the axial power in the minor pattern, whichever is least. It is to be noted that this indicates the maximum usable pattern for fixed-array applications where elliptical polarization is desired. A disadvantage of this representation is the loss of correlation between beamwidth and directivity.

Frequency bands over which the antenna exhibits a linearly polarized beam are indicated by shading of the graphs. In these regions, the beamwidths indicated are those of the major (and only) pattern.

Ellipticity is represented in the form of "axial ratio". Axial ratio is defined as the ratio of the maximum radiation electric field on the helix axis to the minimum radiation electric field. This ratio does not vary significantly over the usable beamwidth if the pattern is symmetrical.

Impedance is plotted on a Smith chart having impedances normalized to fifty ohms.

7. The Concentric Array.

The usual bandwidth of the axial mode is of the order of 1.6 to one. The proposed array is designed to cover adjacent bandwidths using two helical antennas. This indicates the dimensions of the smaller helix should be scaled by a factor of 0.625 to those of the larger. The right circular cylinder envelope of the helices suggests coaxial nesting to reduce the bulk. Inasmuch as the factor of 1.6 approaches two (the accepted diameter ratio of a non-interfering cavity-enclosure), it was initially assumed that the helices would show negligible mutual coupling. If this assumption were to prove true, the use of passive filter networks would allow the desired wide-open operation of the array.

Preliminary studies at Stanford Research Institute indicated termination of the helices at opposite radials from the array axis. Termination of the feed-ends of the two helices in close proximity produced serious coupling between the antennas with resultant poor patterns and ellipticity. The increased separation of the lower turns (due to termination in opposition) decreased this coupling markedly. This can be explained in terms of the greater current magnitudes present in the initial turns of the helices.

8. Results of Measurements.

A. The Three-Turn Helical Antenna.

The radiation pattern of the three-turn helical antenna was investigated. The results are graphed in Figure 5. The dimensions given correspond to a pitch angle of 13.5°. The frequency range of investigation was sufficient to include patterns outside the R_1 mode at either extreme. Thus, while serving as a model for pattern characteristics throughout the beam mode, these results indicate typical patterns of the R_0 and R_2 modes.

The axial beam (R_1) mode extends from 0.66 f_n to about 1.44 f_n. Pattern beamwidths are of the order of 60° over this frequency range, decreasing quite noticeably at the high end due to the increasing electrical dimensions of the radiation aperture. Axial ratios of less than two are recorded from 0.77 f_n to 1.44 f_n. The patterns below 1.0 f_n are nearly circularly symmetrical about the helix axis. Above this frequency, the axis symmetry becomes elliptical with greater radiated power in the $\phi = 90°/270°$ plane. At about 1.4 f_n, the pattern becomes assymmetrical due to tilt.

The normal, (R_0), mode was recorded at 0.51 f_n. This pattern was a conical type, having aggravated axis assymmetry. The pattern was generally normal to the helix axis except for an elevation due to the ground plane. While elliptic polarization was present in the plane of $\phi = 60°/240°$, the ϕ and θ fields of other axial planes (i.e., planes which contain the helix axis) appeared to lack the time quadrature necessary for ellipticity.

The R_2 mode occurs when the circumference of the helix approaches two wavelengths. The pattern for this mode was recorded at 1.7 f_n.

The pattern is conical with a null in the axial direction. The ϕ and θ fields are nearly in time quadrature, giving elliptical polarization in all axial planes. The circular symmetry about the helix axis is somewhat irregular.

The impedance characteristics of this helix are shown in Figure 6. The Smith chart plot is normalized to a characteristic impedance of fifty ohms.

At frequencies below 0.55 f_n, the measurements show the high impedances of the normal (R_0) radiation mode. It is noted that, while the impedance below 0.66 f_n exhibits a fairly constant, high, standing-wave ratio, the helix is not analogous to a short, open-end, transmission line in that the phase of the impedance does not vary in a simple manner with frequency.

The characteristic helical grouping of the axial beam mode impedance is noticed at frequencies above 0.7 f_n. The average impedance of this mode is 77 - j48 ohms. For the frequencies of the R_2 mode, the impedance is very nearly a constant at 58 - j58 ohms. The impedances of the R_1 and R_2 modes will match to an 105-ohm line with a voltage standing-wave ratio (VSWR) less than three.

B. The Three-Turn Scaled Array.

In considering the concentric helix array, it was felt that an optimum filter network should have characteristics capable of being represented by a terminal network incorporating to a two-pole, double-throw switch. This equivalent is shown in Figure 7. The switch position is determined by the frequency of the signal under consideration, being in position one for frequencies of beam operation of the larger helix, and

in position two for frequencies above this. The impedances of Z_1 and Z_2 depend on the filter characteristics and are parameters yet to be determined. If no mutual coupling is assumed, the patterns of the array would be those of the axial beam modes and the array would cover an approximate bandwidth of $(1.6)^2$ or 2.56.

The next array examined (Figure 8) represents this configuration where the switch is in position one. The smaller antenna is scaled for the next higher band of frequencies by a scaling factor of 0.625. This antenna is connected directly to the ground plane by an electrically short ($h = 0.13\ D_1$) stub. This is equivalent to an extremely small terminal impedance, i.e., an effective short circuit.

The radiation patterns of this configuration are very similar to those of the single helix. The lower axial-beam-mode extreme was lowered slightly. Axial ratios were comparable to those of the single helix. Beamwidths were increased for all frequencies below 1.0 f_n.

The impedance plot of this configuration is shown in Figure 9. The plot again shows high impedances for the normal (R_0) mode, and the characteristic helical grouping for the R_1 and R_2 modes. Comparison with the impedance plot for the single helix indicates very similar imput impedances. The average terminal impedance of the R_1 mode is 110 - j30 ohms. The R_2 mode impedance is very nearly constant at 120 - j32 ohms. Both modes may be matched to an 145 ohm line with a VSWR less than three.

The foregoing measurements indicate that the mutual coupling between the antennas is small when the larger helix is operating in the axial beam mode and the smaller is below this mode.

The third array examined represents the optimum filter configuration where the switch is in position two. The smaller helix is driven while the larger is effectively short-circuited to the ground plane. The shorting-stub length is electrically small.

The radiation patterns of this configuration were unacceptable. As indicated in Figure 10, only the extremes of the frequency band produced usable patterns. At the low end, beamwidths were narrow due to the broad electrical aperture of the outer parasite and large minor lobes were present. At the approximate mid-frequency range, 1.6 f_n, the reradiated R_2 pattern of the parasite dominated the radiation. This domination decreased with increasing frequency but was present and appreciable at 2.0 f_n.

C. Unbalanced Scaled Array.

This violent interaction between the R_1 and R_2 modes (multimoding of the array) is in direct contradiction to the initial assumption of negligible mutual coupling between the antennas. To reduce this coupling, the outer helix was reduced to 1-7/8 turns. This makes the axial lengths of the two helices equal. In this manner, it was thought to reduce the scattering effect of the extreme turns of the parasite[1] and to reduce the permissible resonant lengths.

This array (Figure 11a) produced narrow but usable beamwidths (approximately 30°) at frequencies above 1.4 f_n. Axial ratios were generally less than two. However, all patterns exhibited approximately 20° tilt of the minor pattern, usually in the $\phi = 0°$ half-plane, indicating noticeable mutual coupling. In an effort to further reduce coupling,

[1]P. Ferrer and E. S. Akely, Scattering of Electromagnetic Radiation by a Thin Circular Ring, J. Appl. Phys., 19, pp. 39-46, January, 1948.

the outer antenna was mounted on the ground plane by means of a high-frequency mounting capacitor (Figure 11b). This changes the impedance, Z_1, to a capacitive reactance. This change in the terminal impedance of the parasitic antenna produced no appreciable change in the radiation patterns of the array.

D. 1 1/4-Turn Scaled Array.

To avoid the narrow beamwidths prevailing throughout the operating region of the smaller helix, both antennas were reduced to one and a quarter turns. It was expected that the decreased axial length of the array would also decrease the mutual coupling.

Both helices were radius-and-loop loaded to improve their axial-beam characteristics. This loading is a small loop about the helix axis connected to the open-end of the helix by a radial conductor. Its purpose is the change of the reflection coefficient of the open-end of the helix to diminish the reflected wave.

The first array (Figure 12) corresponds to the high-frequency optimum filter equivalent. These patterns are approximately twice as wide (average beamwidth of 60^{o}) as the three-turn array. Axial ratios are reasonable except at the lower end of the high frequency band. The tilt of the minor pattern is not as excessive as previously noted, but, the axial assymmetry of the major pattern is more pronounced than before. Variations of the terminal impedance of the outer helix, Z_1, did not produce any significant change in the radiation patterns.

The array was then jointly fed from a single axial feed (Figure 13) through radius feed sections having characteristic impedances of

approximately 85 ohms.[1] This arrangement is closely modeled to the most promising of the arrays considered by Stanford Research Institute in 1955.

The improvement in radiation-pattern characteristics was greater than could be expected on the basis of prior optimum filter results. The array has an acceptable bandwidth of about 2.2 to one. Average beamwidths of about 50° are realized with very slight narrowing at the upper end of the operating region. Axial ratios are generally less than three, except for frequencies near 1.5 f_n. Almost all pattern improvement is accompanied by an increase in pattery symmetry (and a decrease in tilt) over that of the optimum filter equivalents.

E. Equal-Spacing Array.

Additional decoupling was sought using helices having scaled diameters ($F = 1.6$), but having equal spacing ($S_1 = S_2 = 0.716\ D_1$). These dimensions correspond to pitch angles of 12.9° for the larger helix and 20° for the smaller. The separation of the conductor cross-sections of the large and small helices is maximum in any axial plane.

The radiation patterns of this array (Figure 14) were a significant improvement over previous arrays. The minor pattern showed good symmetry with the array axis. Some assymmetry of the major pattern is noted at frequencies above 1.4 f_n. Large minor lobes appear at 2.25 f_n, becoming more dominant with increasing frequency. Beamwidths of 40° are

[1]The characteristic impedance of a circular conductor above a ground plane is given by:

$$Z_0 = 60 \cosh^{-1} (h/b)$$

where h is the distance between the ground plane and the conductor center and b is the conductor radius. This expression neglects ohmic and radiation losses.

obtained over most of the frequency band. Axial ratios are less than 2.5 from 0.9 f_n to 2.3 f_n. This gives a usable bandwidth of about 2.5 to one.

An additional slug load ($l_s = 0.65\ D_1$) was added, common to both antennas. This is shown in Figure 15. This loading improved beamwidths to about 55° except at the very high end of the frequency band. Axial ratios are less than two for a bandwidth of 2.4, from 0.92 f_n to 2.2 f_n. Some tilt is noted at frequencies above 1.4 f_n, but this effect does not radically affect the minor pattern of circularly polarized fields. The minor lobes appearing at 2.25 f_n are more pronounced than before and become excessive at higher frequencies. Variations of the slug length did not change the magnitudes of the lobes appreciably.

An increased helix-diameter ratio (F = 1.95) gave a marked deterioration of the radiation-pattern characteristics. Characteristics of corresponding arrays are plotted in Figure 16 and Figure 17. The radiation patterns for frequencies about 1.7 f_n are linearly polarized. Above 1.5 f_n, tilt of the minor pattern was excessive with a median value of about 20°. This, in a large measure, is responsible for the apparent erratic behavior of beamwidth and axial ratio with frequency.

F. Helices in a Cavity.

Cavity enclosure of the 1.6-scaled array was investigated. The enclosure is a brass cylinder having an inside diameter twice the outside diameter of the array (Figure 18). The depth of the cavity (h_c) is variable.

The array of Figure 14 was mounted at maximum cavity depth, $h_c = 1.5\ D_1$. The patterns (Figure 19) showed a more narrow, average beamwidth due to the increased radiation aperture of the cavity. The

circular symmetry of the major pattern was good. Tilt of the minor pattern at mid-range frequencies increases axial ratios to about 2.6. The usable bandwidth is about 2.3 to one.

When the array is mounted at minimum depth, h_c equal to the axial length of the array, and the larger helix is slug-loaded ($l_s = 0.39\ D_1$), an improvement of the low-frequency characteristics is noted (Figure 20). The patterns display greater axial symmetry over the 2.5 to one bandwidth. Axial ratios are less than two except at frequencies near 1.6 f_n. Beamwidths show characteristic decrease from 60° at the lower frequencies to about 35° at the highest frequencies.

Integrated directivities of this array were approximately six decibels over a linearly-polarized, isentropic antenna for radiation fields at low, medium, and high frequencies of the operating band.

Input impedance measurements of this array (Figure 21) indicate band of slowly varying impedance from 0.8 f_n to 1.1 f_n, and from 1.3 f_n to 2.1 f_n. Input resistance varies from 25 to 70 ohms while reactance values are less than 50 ohms. The array will match a 50 ohm line with voltage standing-wave ratios less than three.

One turn helical arrays produced similar results for the lower frequencies of operation (Figures 22 and 23), but excessive tilt was observed above 2.0 f_n.

G. Top-Loading Effects.

Investigation of top-loading of the one and a quarter-turn array was conducted at the center-frequency region having poor axial ratios. The helical slug[1], (a uniform helix of six turns whose diameter is 1/6 D_1

[1]Springer, loc. cit.

and whose axial length is 1/3 D_1) gave the best improvement of axial ratios, with values of about two. Axial ratios of about 2.2 were obtained with loop and radius loading when the diameters of the loops were about four-tenths the diameters of the respective helices. This dimension was not sharply critical. Loops much larger than this produced electromagnetic scattering while smaller loops resulted in poorer axial symmetry. The ease of manufacture of the loop and radius is a significant advantage.

H. Cross-Wound Helices.

The radiation patterns of a cavity-enclosed, concentric array having cross-wound helices, Figure 24, show a definite decrease in mutual coupling. The low-frequency helix is fed through a two-section low-pass filter. Both major and minor pattern symmetry is good below 2.1 f_n. However, at the cross-over frequency of the antennas of this cross-wound array, linear polarization must be expected because of the opposite senses of the two helices.

9. Tilt.

Tilt is the off-axis location of the maximum field of a beam antenna. It is usually accompanied by assymmetry of the radiation pattern. A model explaining this behavior is easily developed through consideration of even and odd mode radiation patterns.[1]

To outline this model let us consider the radiation patterns of two radiating horns placed side-by-side in the H-plane. When the aperture electric fields are equal and in-phase, the radiated energy is concentrated in a large main lobe.[2] This is illustrated in Figure 25a. The equal and in-phase fields will be called the even mode.

Next, consider the case where the fields of the apertures are equal, but are in phase opposition. As shown in Fibure 25b, the radiation pattern will suffer cancellation on the array axis, and the radiation pattern will consist of an even number of lobes, symmetrical with the array axis. For purposes of illustration, the number will be taken as two. These lobes differ in sense and may be said to be 180° apart in phase. This aperture distribution will be called the odd mode.

If the radiated powers of the horns are equal, but in phase quadrature, we can consider an instant of time where the even mode alone is present. This is represented in phasor notation in Figure 25c. Similarly, from the field distribution three-quarters of a cycle later, only the odd mode will be present, as is shown in Figure 25d.

[1]Dr. T. Morita introduced this concept in a private discussion at Stanford Research Institute in March, 1957.

[2]Kraus, op. cit., p. 36.

In phasor notation, we may then write,

(1) $\bar{E}_e = \bar{E}_1 + \bar{E}_2$,

and (2) $\bar{E}_o = \bar{E}_1 - \bar{E}_2$, where $\bar{E}_1$ and $\bar{E}_2$ are the phasor representation of the aperture fields of horns 1 and 2 respectively, and $\bar{E}_e$ and $\bar{E}_o$ are the phasor representation of the even and odd modes respectively.

If the fields, $\bar{E}_1$ and $\bar{E}_2$, have arbitrary values, such that,

$\bar{E}_1 = x_1 + j\, y_1$,

and $\bar{E}_2 = x_2 + j\, y_2$, then the even and odd modes are:

$\bar{E}_e = x_1 + x_2 + j\,(y_1 + y_2)$

and $\bar{E}_o = x_1 - x_2 + j\,(y_1 - y_2)$.

For non-interference between the radiation patterns of the even and odd modes, the patterns associated with each must be in time quadrature (or one or both of the magnitudes must be zero.) For time-quadrature to exist,

$\bar{E}_e = \pm\, jk\bar{E}_o$.

This may be written,

$$x_1 + x_2 + j(y_1 + y_2) = \pm\, jk(x_1 - x_2) \mp k(y_1 - y_2).$$

Equating real and imaginary quantities,

$$x_1 + x_2 = \mp\, k(y_1 - y_2)$$

$$x_1 - x_2 = \pm\, \frac{1}{k}(y_1 + y_2).$$

$$\pm\, x_1 = \frac{1 - k^2}{2k}\, y_1 + \frac{1 + k^2}{2k}\, y_2$$

$$\mp\, x_2 = \frac{1 + k^2}{2k}\, y_1 + \frac{1 - k^2}{2k}\, y_2$$

$$|E_1|^2 = x_1^2 + y_1^2 = \frac{1}{4k^2}\left[(1 - 2k^2 + k^4)\, y_1^2 + (1 - k^4)\, y_1 y_2 + (1 + 2k^2 + k^4)\, y_2^2 + 4k^2 y_1^2\right]$$

$$= \frac{1}{4k^2}\left[(1 + 2k^2 + k^4)\,(y_1^2 + y_2^2) + (1 - k^4)\, y_1 y_2\right]$$

$$|E_2|^2 = x_2^2 + y_2^2 = \frac{1}{4k^2}\left[(1 + 2k^2 + k^4)\, y_1^2 + (1 - k^4)\, y_1 y_2 + \right.$$
$$\left. + (1 - 2k^2 + k^4)\, y_2^2 + 4k^2 y_2^2\right]$$

$$= \frac{1}{4k^2}\left[(1 + 2k^2 + k^4)\,(y_1^2 + y_2^2) + (1 - k^4)\, y_1 y_2\right]$$

$$\therefore \; |E_1| = |E_2|$$

Therefore, it is seen that the condition for symmetrical fields in the presence of multimoding is equal aperture fields, (i.e., $|E_1| = |E_2|$).

Where this time quadrature of the odd and even modes does not exist, it is beneficial to examine the radiation patterns for that instant of time when the even mode has its maximum value. The instantaneous even mode pattern will be the single main lobe shown in Figure 26a. The instantaneous (in time phase with the even pattern) odd mode pattern will be a double-lobed pattern. The magnitudes of the lobes will be proportional to the vertical component of $\bar{E}_o$. One of the radiation lobes will have the same sense as the lobe due to $\bar{E}_e$ while the other will have an opposite sense. This is illustrated in Figure 26b.

Superposition of the two radiation patterns gives reinforcement of the fields on one side of the axis and cancellation on the other. When the fields of the two modes are of comparable values, the direction of the maximum average field will no longer lie on the axis but will have an off-axis position. This resulting tilt is shown in Figure 26c.

In applying this model to the helix, the axial beam mode will be considered the even mode.

There are several odd modes to be encountered in the helix. These odd modes include the R_0 and R_2 mode but the most important is a mode exclusive to the concentric array. This mode is best demonstrated by two identical helices fed in phase but with terminations in axial opposition to each other (see Figure 27). Examination of the axial radiation

pattern indicates that any current element in one helix contributing to the axial field will be opposed by an equal and opposite contribution from the other helix, due to the axial symmetry of the array. This gives exact cancellation of the radiated pattern in the axial direction. The resulting pattern thus is a conical lobe symmetrical with the axis. The traveling wave distribution of currents on a helix indicates that the phase of the pattern must vary with rotation in ϕ.

Measurement of such an array indicated close agreement with the above theory although the conical lobe displayed elliptical symmetry about the axis because of the short length of the antenna used. The fields of this pattern are linearly polarized with the plane of polarization at an angle, α, with the helix axis, i.e., normal to the nearer conductors.

In the concentric array covering adjacent frequency bands, it can be seen that the current distribution of the larger helix must decrease in magnitude with frequency while the magnitude of the smaller helix is increasing. Thus, there will exist a region of cross-over frequencies where the currents are of similar magnitudes but are not equal. To the extent that the concentric array approaches the array of Figure 27, the odd mode of radiation will exist and will interact with the axial beam mode.

10. Summary.

An array of concentric helical antennas scaled for adjacent frequency-band coverage of the axial beam mode exhibits multimoding, i.e., the simultaneous presence of dissimilar modes of radiation. Except in the particular instances where the even and odd modes of radiation are in quadrature, the axial beam patterns are deteriorated. Pattern deterioration due to this multimoding is usually in the form associated with tilt. Tilt, in turn, results in poor axial ratios, poor directivity, and more narrow, usable beamwidths.

Two separate cases of multimoding are distinguished. In the first case, mutual coupling exists between the two antennas at the axial beam frequencies of the smaller. While the radiation of the smaller helix is an even mode, the reradiation of the larger helix is in the R_2 or odd mode. In the second case, when the helices are wound with the same sense, an effective "current-couple" about the helix axis produces an odd mode of radiation peculiar to the array throughout the region of cross-over frequencies. Similarly, this odd mode of radiation interacts with the axial beam or even mode.

The multimoding of the first case may be reduced by reduction of the mutual coupling. This leads to maximum diameter ratios, equal pitch (number of turns per inch) antennas, and, in the absence of other considerations, cross-wound helices. The multimoding in the second case is reduced by destroying the purity of the "current-couple" of the array. This may be done effectively by the employment of cross-wound helices and, to a lesser extent, by greater diameter ratios.

For the coverage of adjacent frequency bands, the diameter ratio is fixed by the bandwidth of a single helix and is insufficient to provide

freedom from multimoding. While the cross-wound helical antenna array does lead to minimal multimoding, the radiation pattern of the array must undergo linear polarization during the transition between the oppositely sensed (clockwise and counterclockwise) antenna operating regions.

While the array covering adjacent bandwidths is highly susceptible to these radiation irregularities, arrays which do not require continuous frequency coverage, and which have antenna diameter ratios greater than two, should be relatively free from such interaction between radiation modes.

The principal effect of a cavity enclosure twice the diameter of the array is a general narrowing of beamwidths due to the cavity aperture. This effect is minimized when the array is mounted at a minimum depth.

Top-loading improves the bandwidth and ellipticity of individual short, helical antennas, but where mutual coupling is present, the magnitudes of induced currents are also increased.

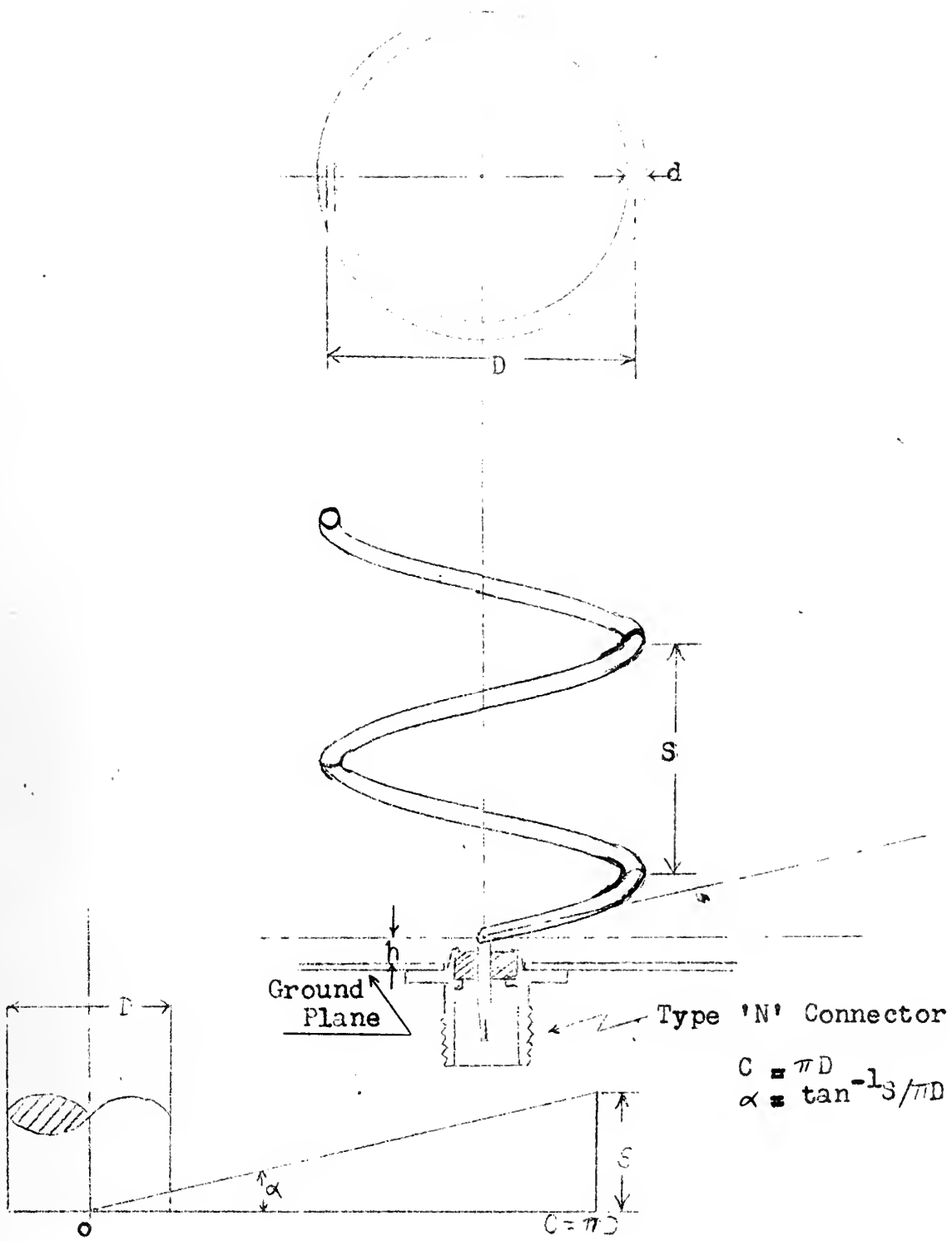

Fig. 1. The Helix Parameters.

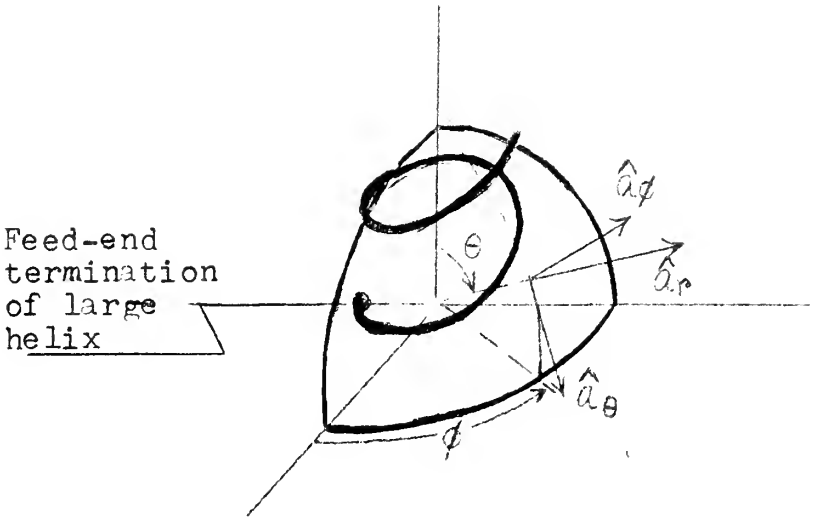

Fig. 2. The coordinate system.

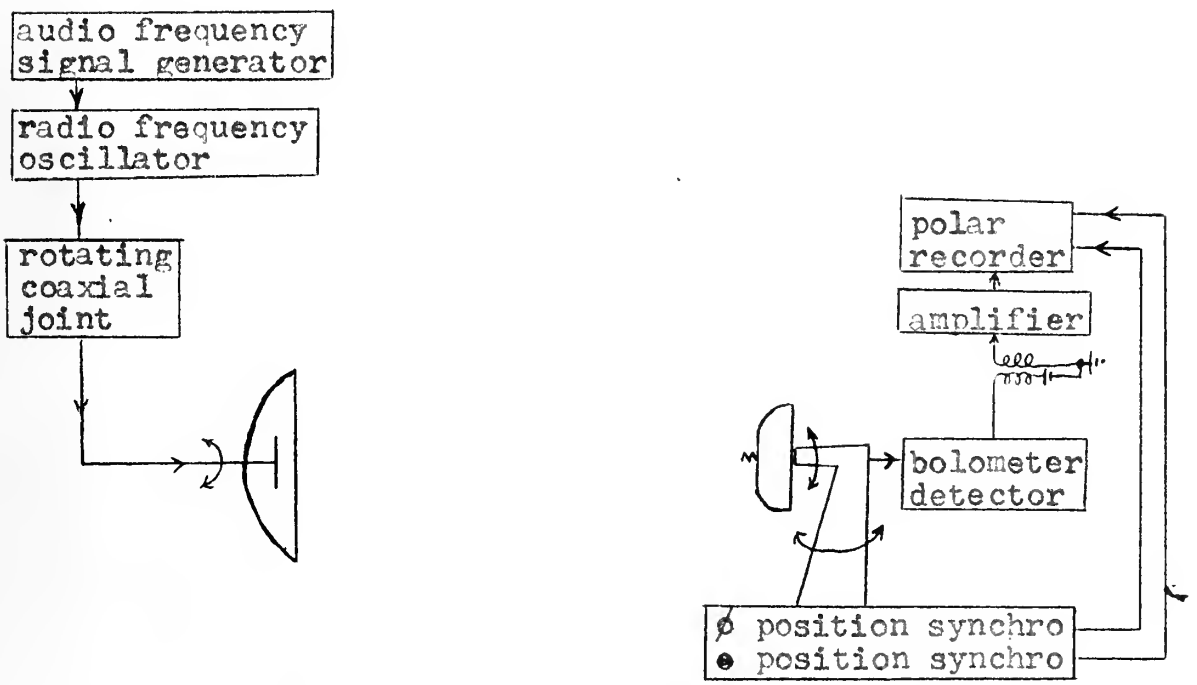

Fig. 3. Pattern Range - Simplified Block Diagram.

FILE NO. _____

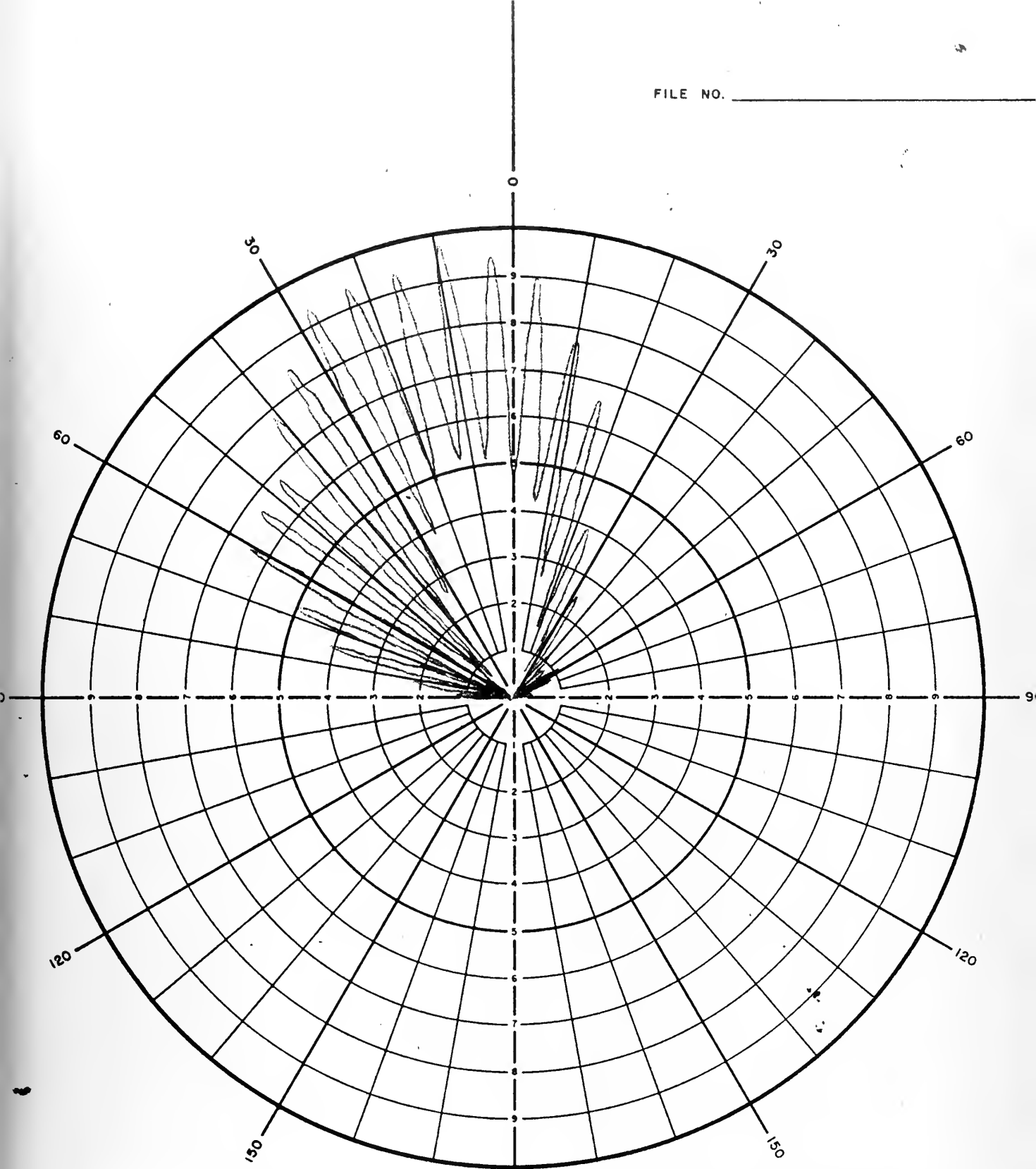

Fig. 4. Power Pattern. Taken with rotating polarization.

C-591

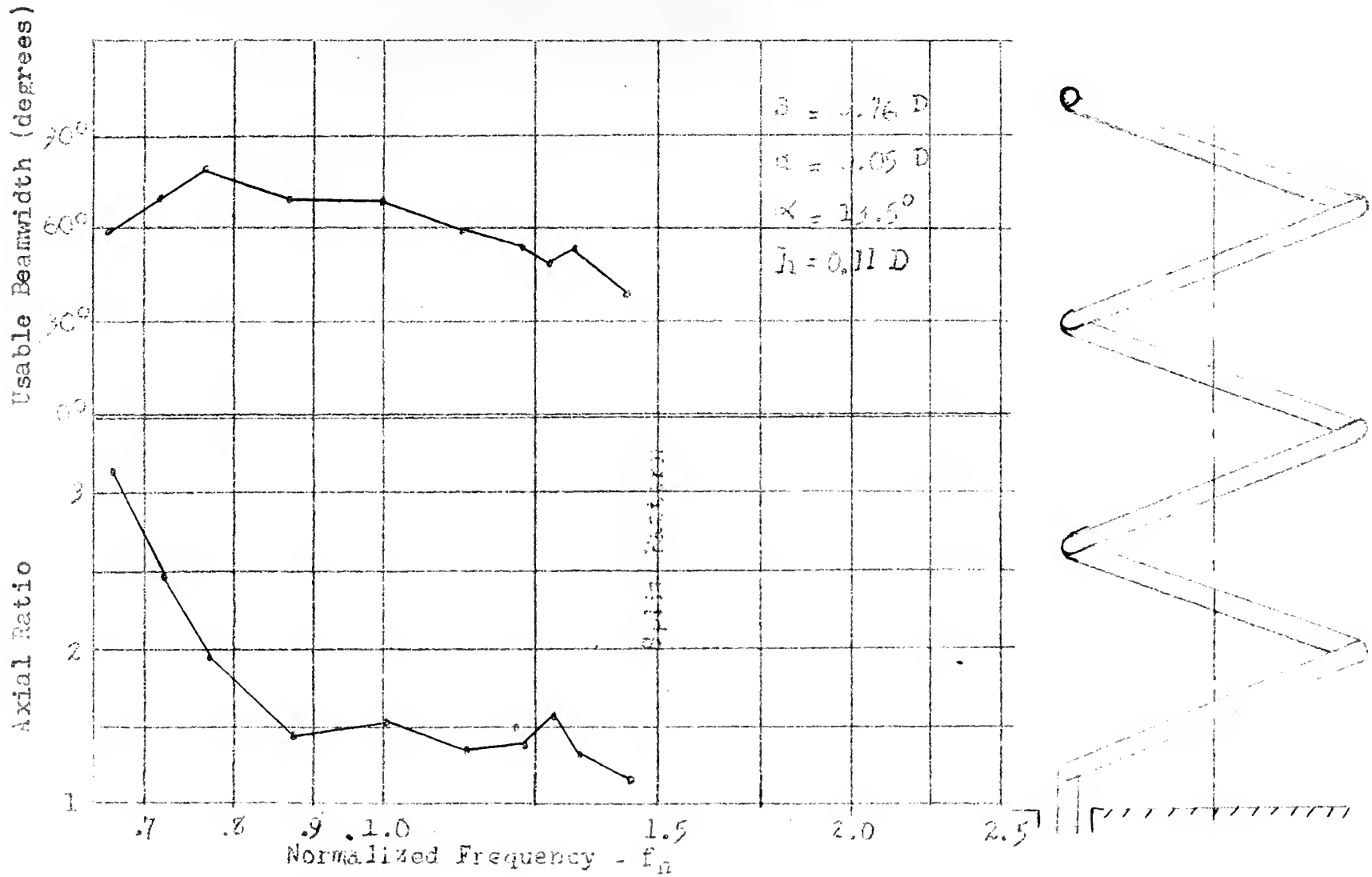

Fig. 3. Measured Radiation Pattern Characteristics of the 14.5°, 3-turn Helix.

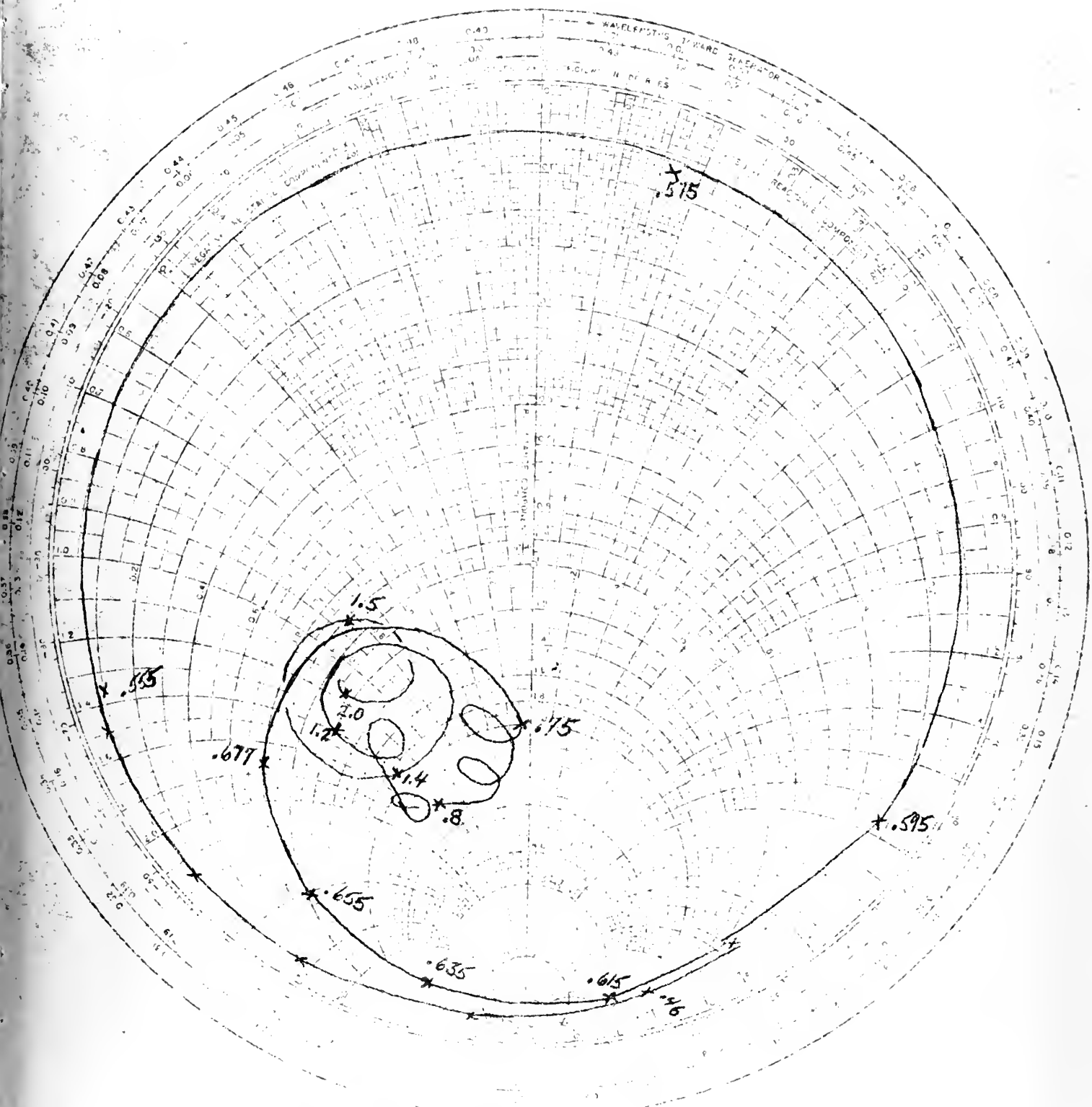

Fig. 6. Measured Impedance of a 13.5°, 3-turn Helix. Z_0 = 50 ohms. Frequencies are normalized.

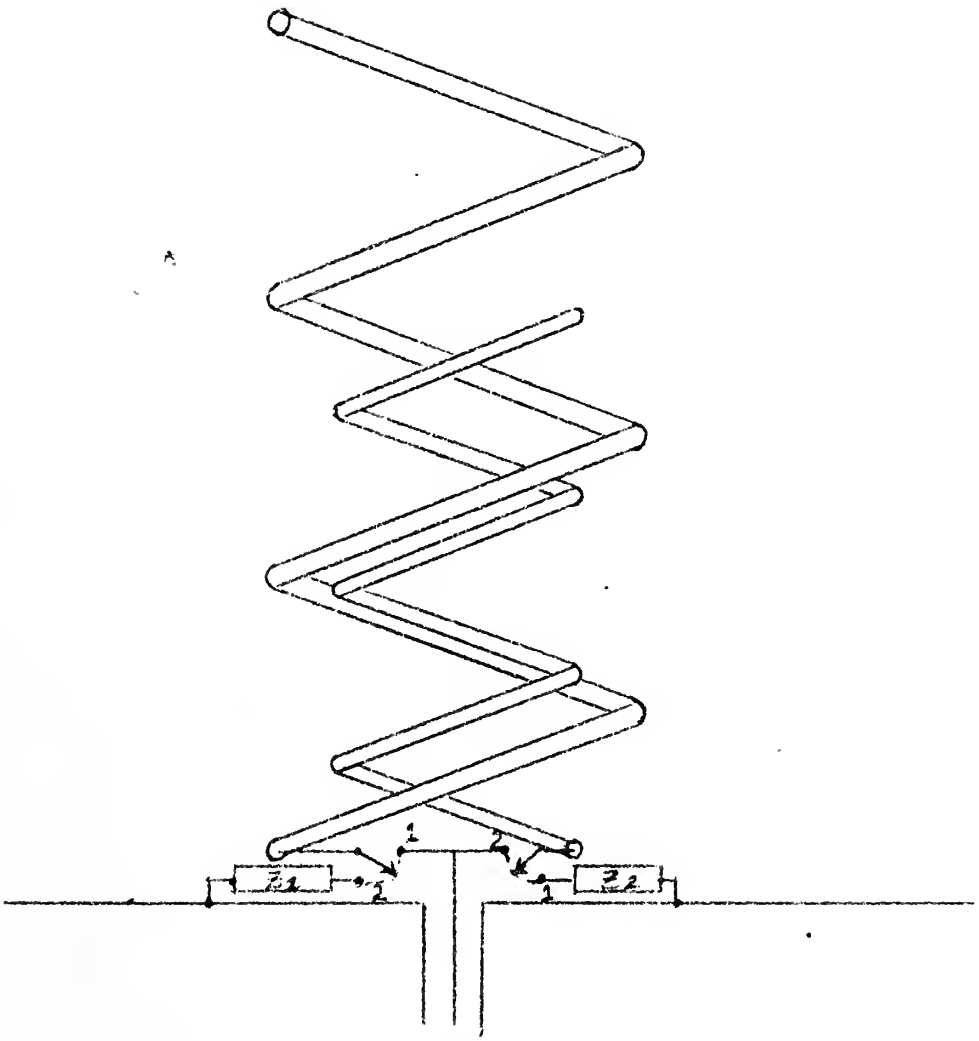

Fig. 7. Illustrative Optimum-Filter Feed for the Concentric Array.

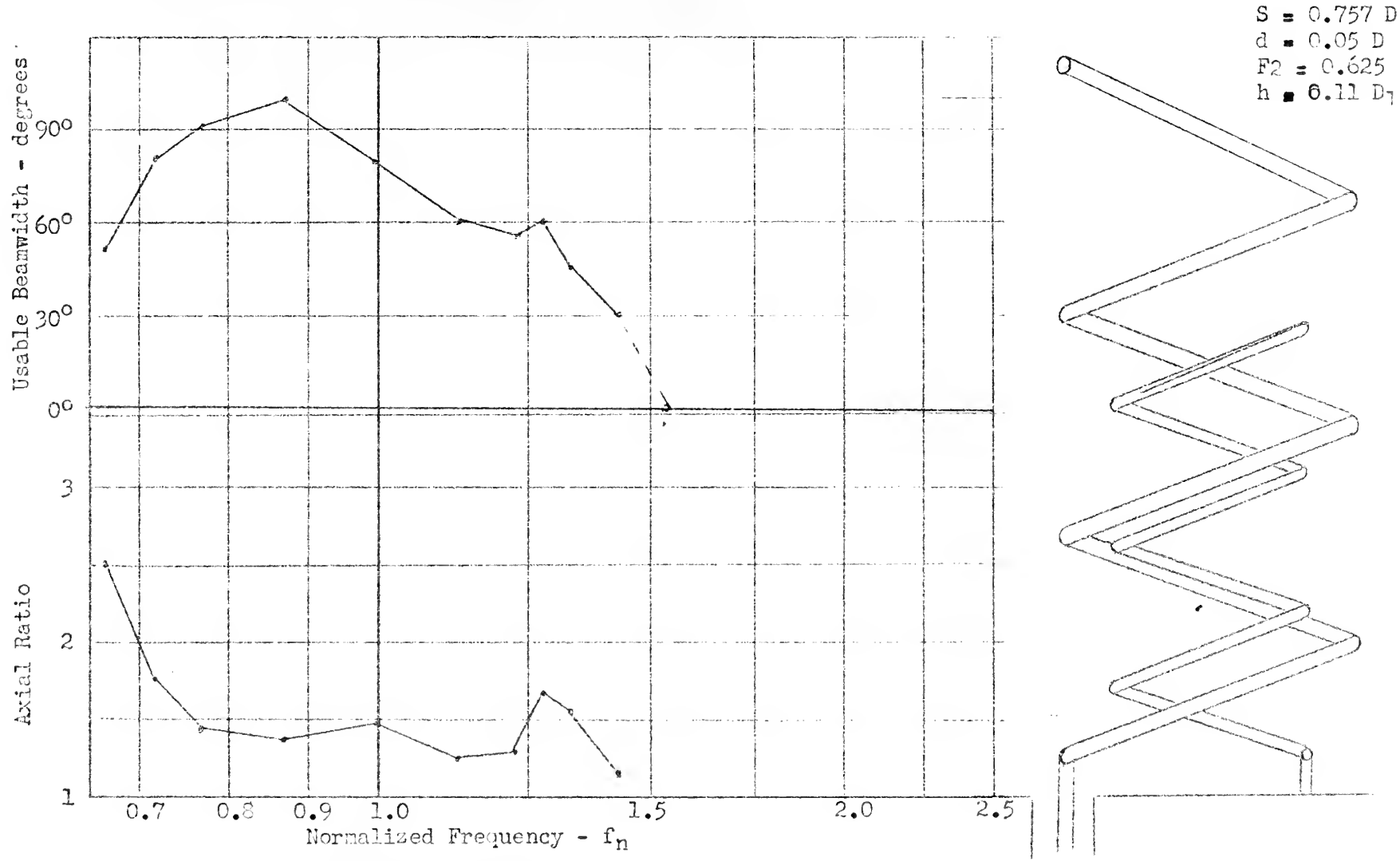

Fig. 8. Measured Radiation Pattern Characteristics of a 13.5°, 3-turn Helix, having a 0.625-scaled parasite.

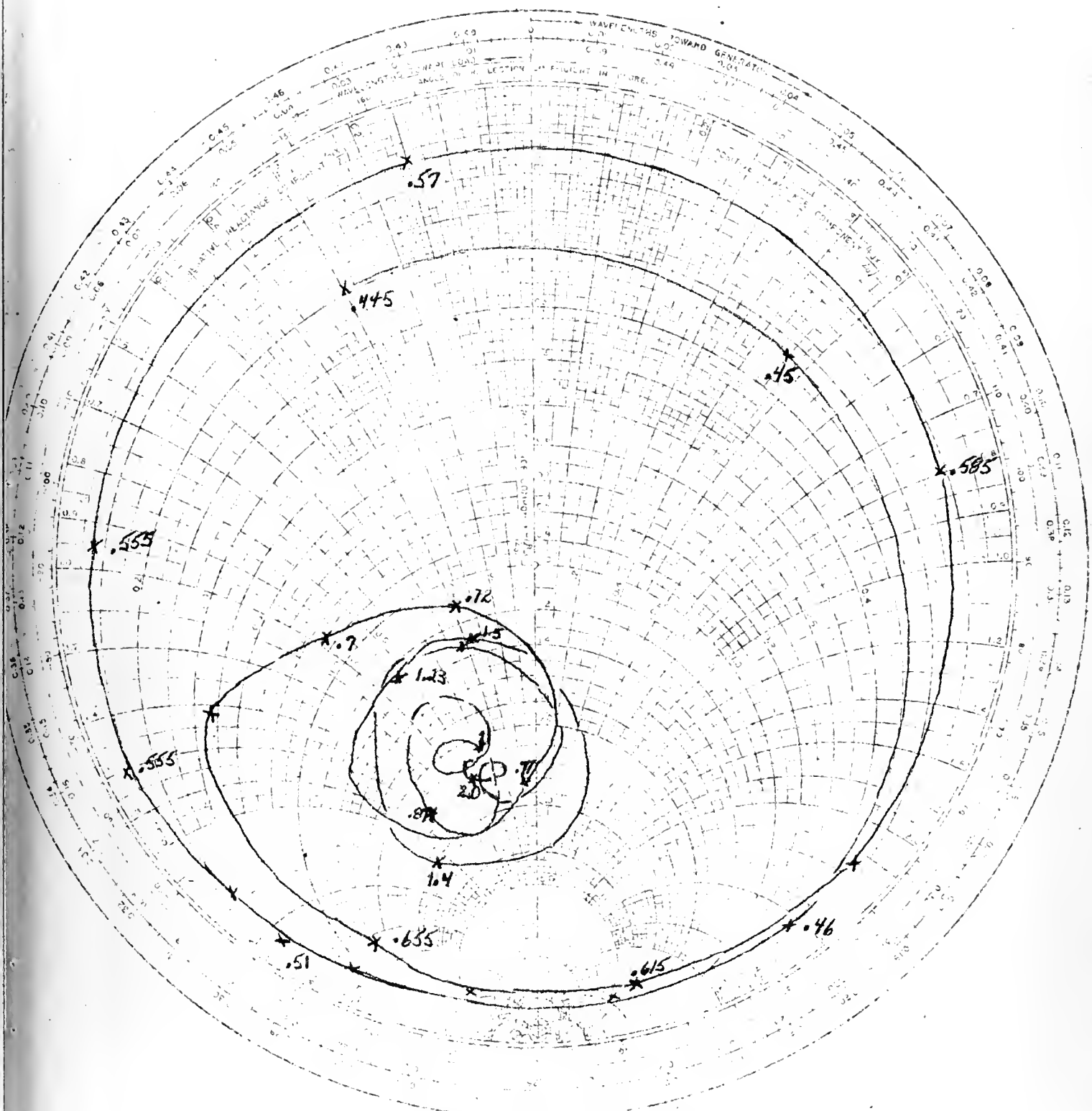

Fig. 9. Measured Impedance of a 13.5° 3-turn Helix, having a 0.625-scaled parasite. Z_0 = 50 ohms. Normalized Frequencies.

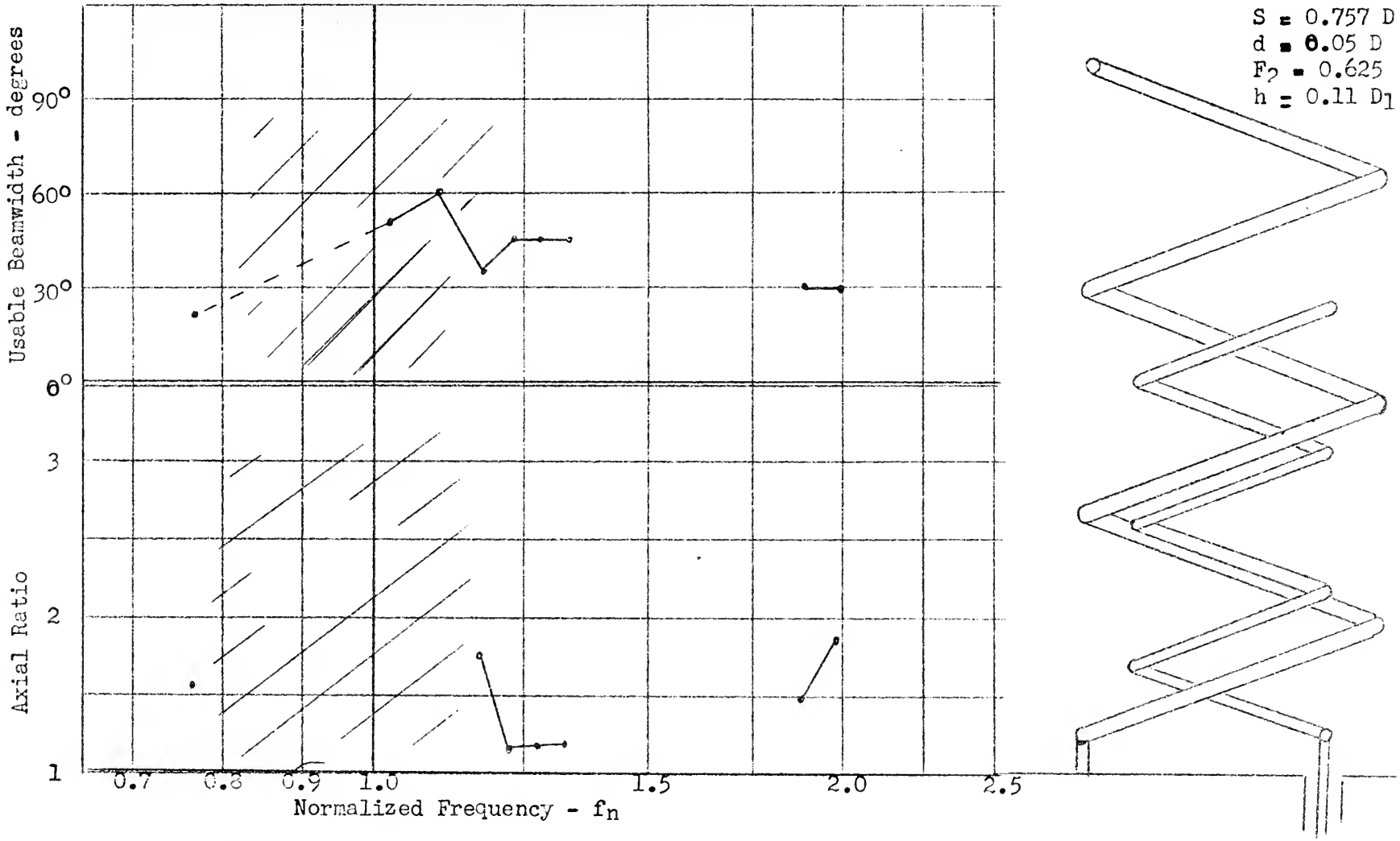

Fig. 10. Measured Radiation Pattern Characteristics of a 13.5°, 3-turn Helix, having a 1.6-scaled parasite.

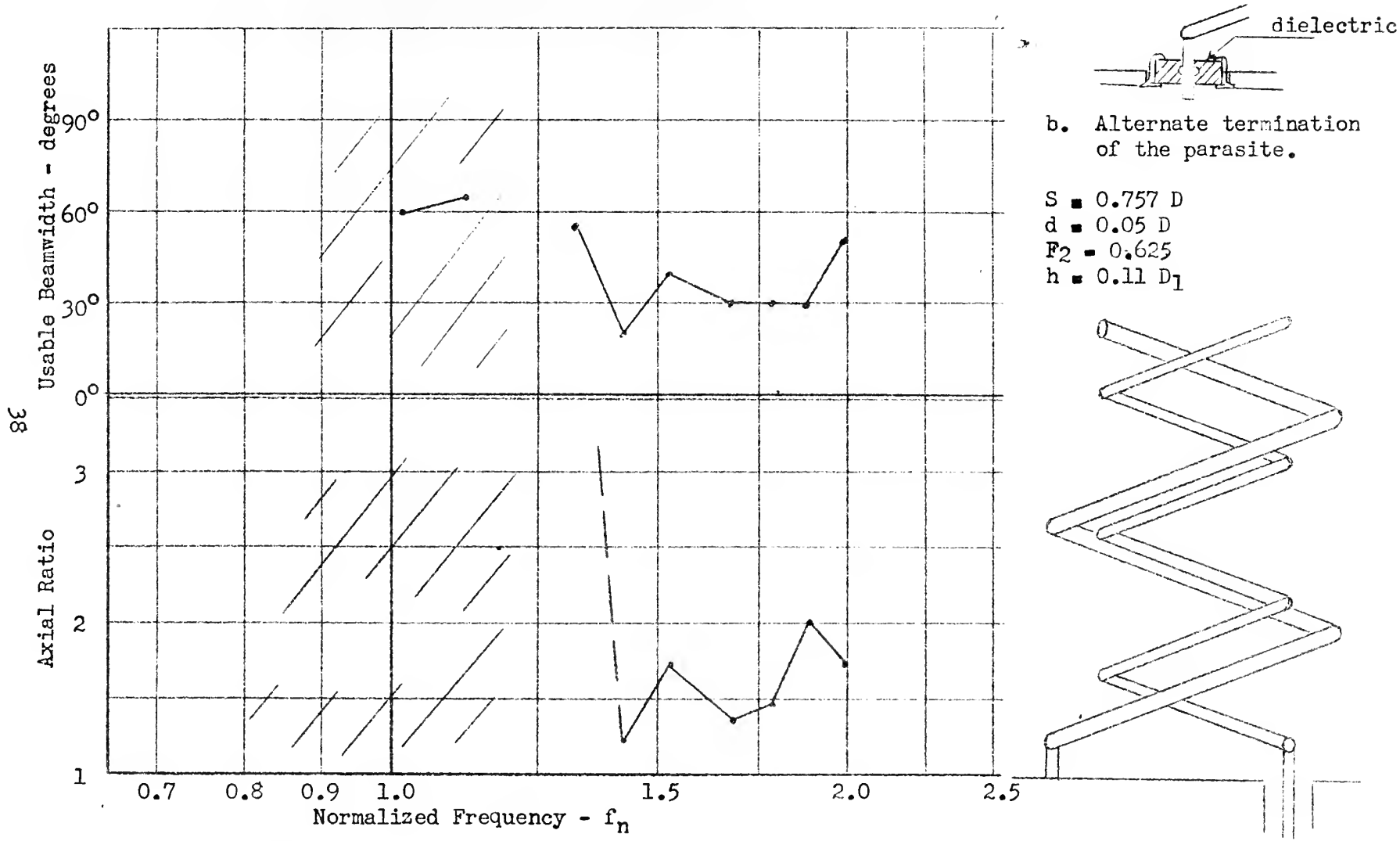

Fig. 11. Measured Radiation Pattern Characteristics of a 13.5°, 3-turn Helix, having a 1.6-scaled, 1 7/8-turn parasite.

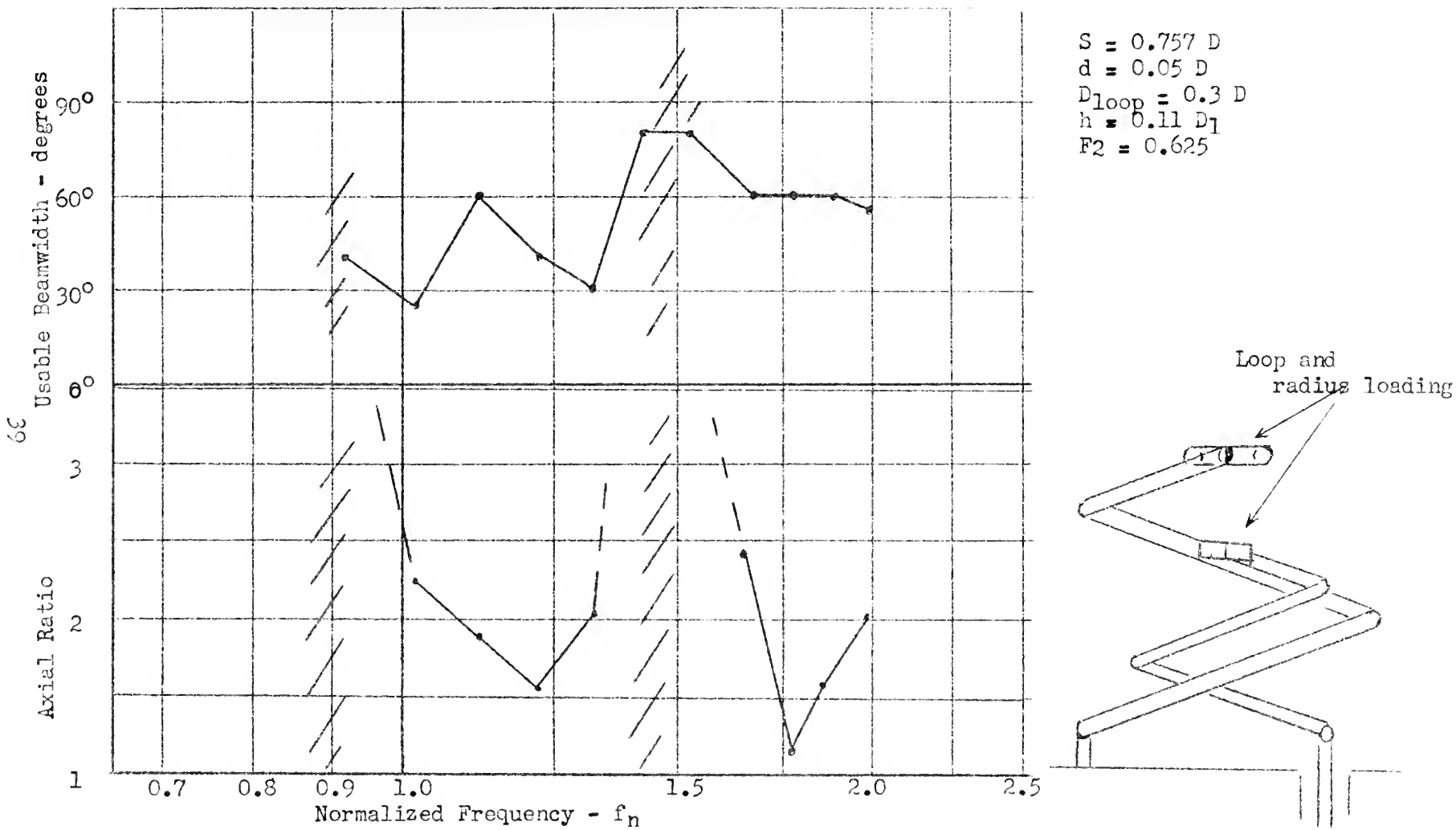

Fig. 12. Measured Radiation Pattern Characteristics of a 13.5°, 1¼-turn Helix, having a 1.6-scaled parasite.

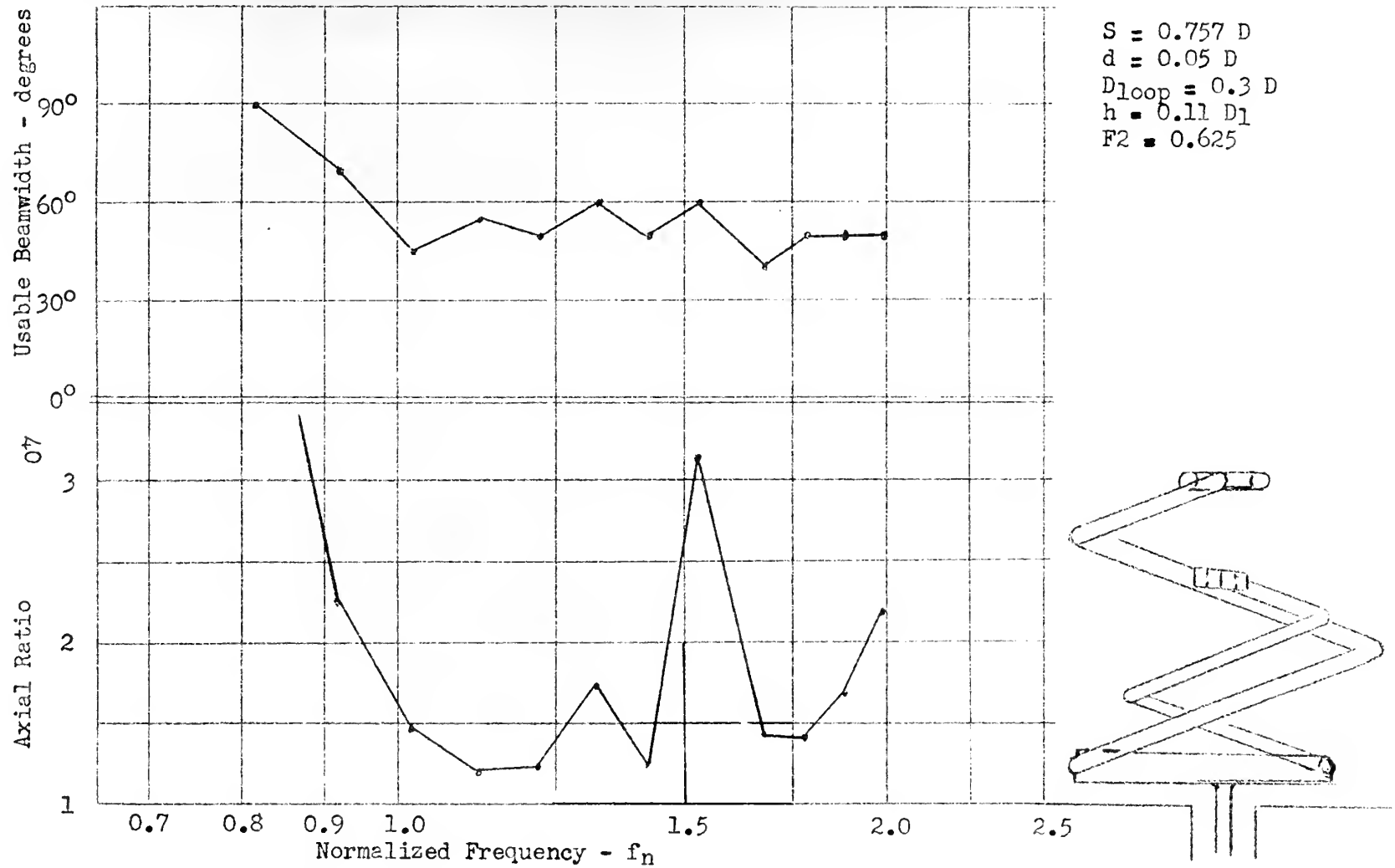

Fig. 13. Measured Radiation Pattern Characteristics of a 13.5°, $1\frac{1}{4}$-turn Array.

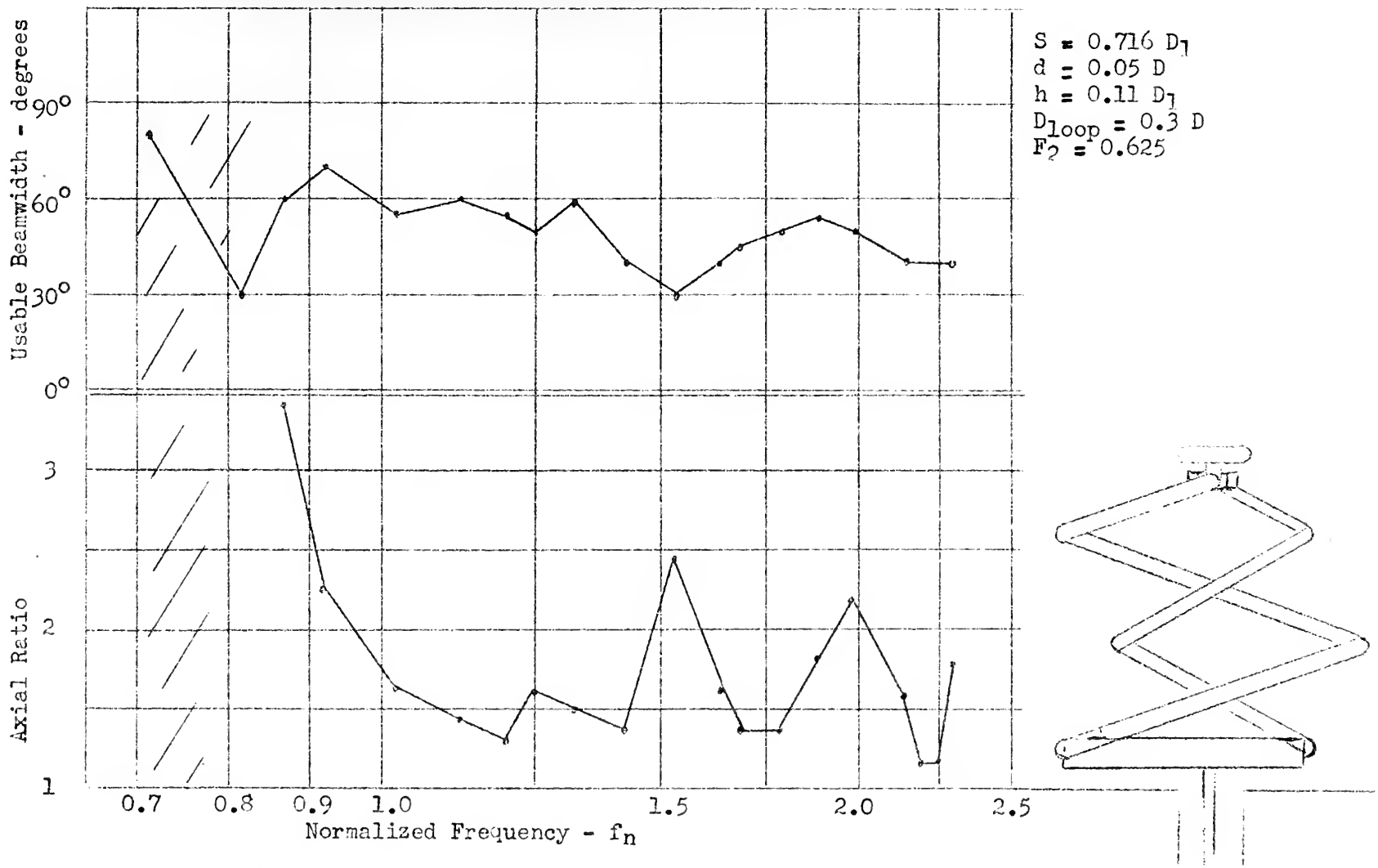

Fig. 14. Measured Radiation Pattern Characteristics of the Equal-Spacing Array.

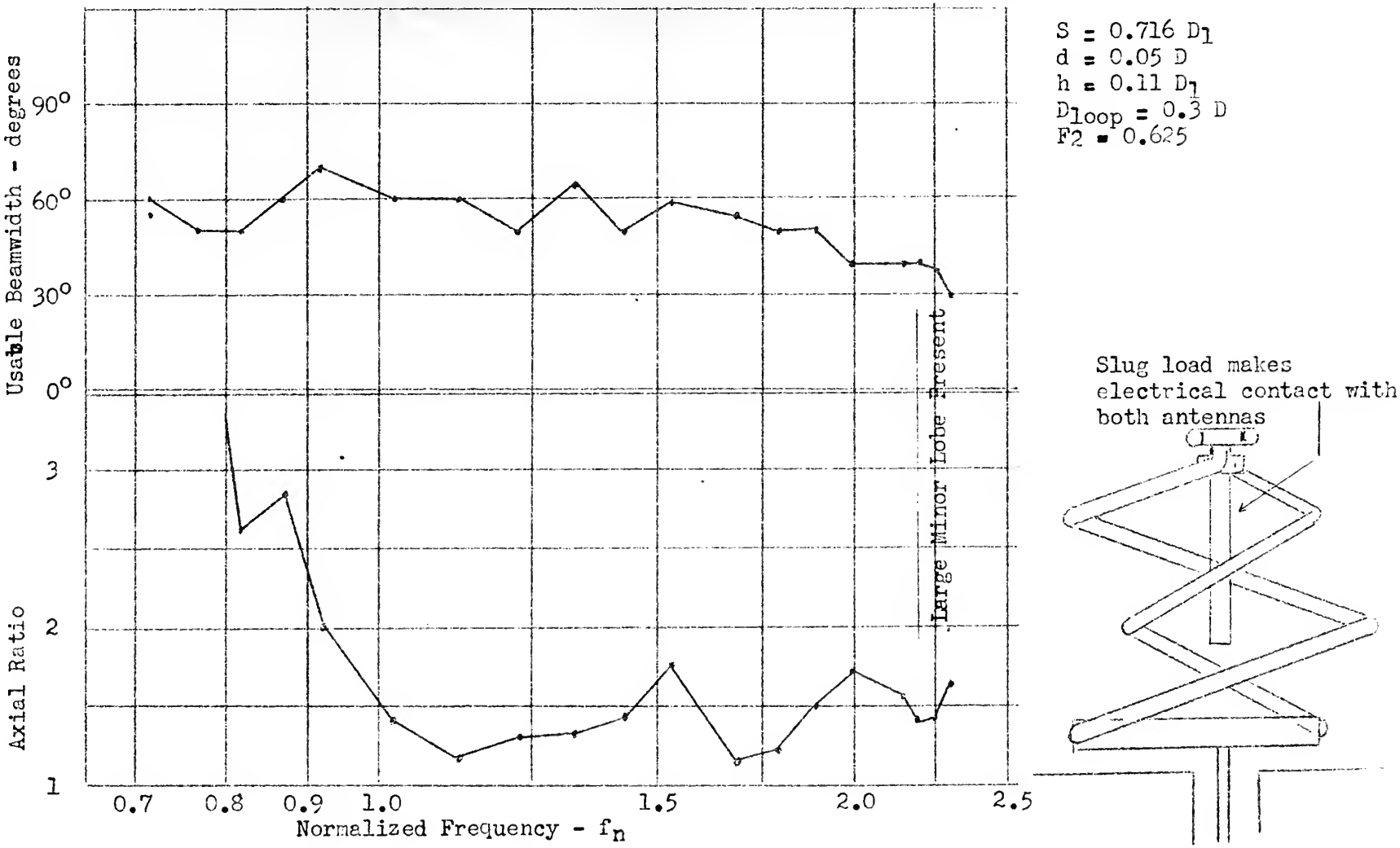

Fig. 15. Measured Radiation Pattern Characteristics of the Equal-Spacing Array (Slug-loaded). Length of Slug = 0.65 D_1.

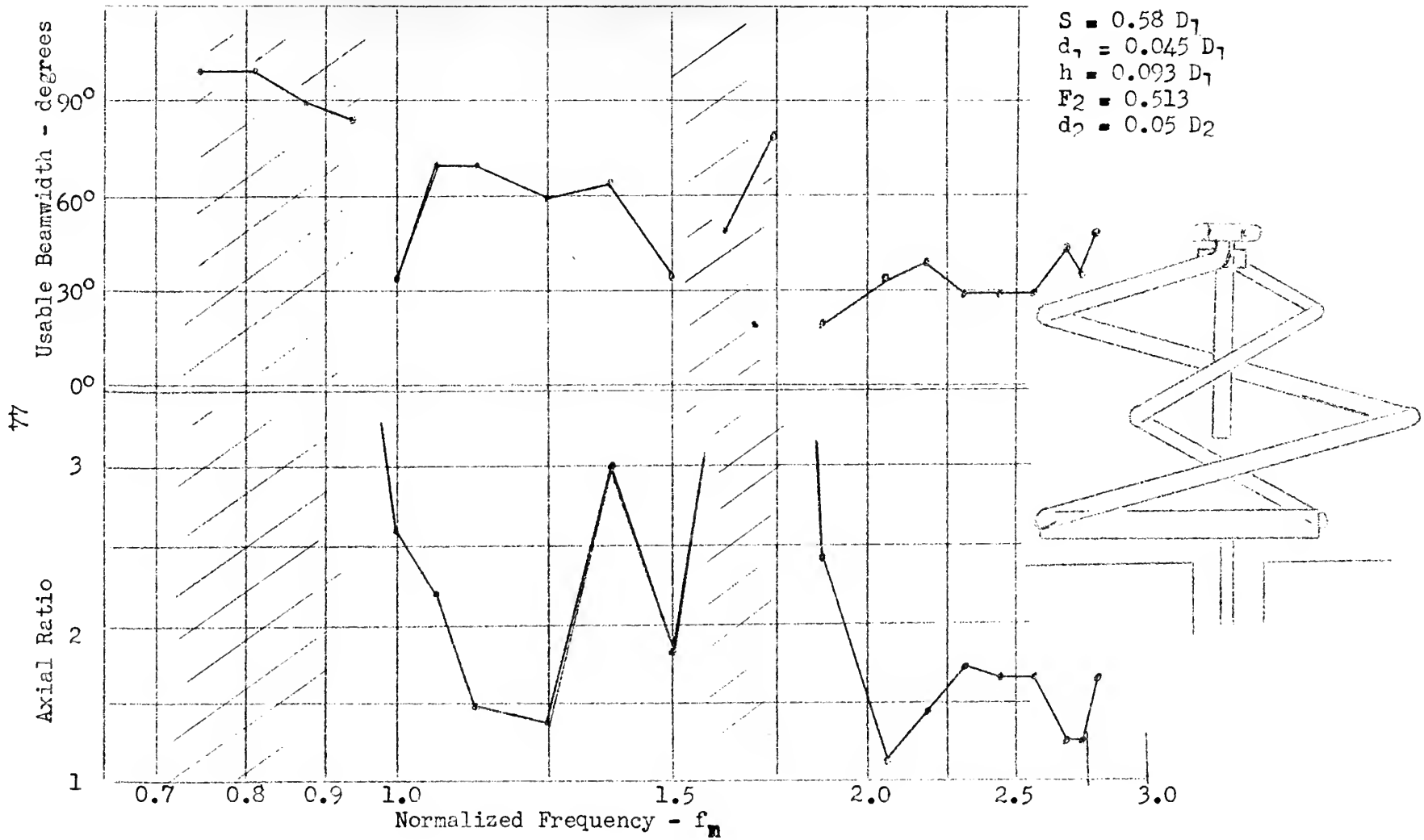

Fig. 17. Measured Radiation Pattern Characteristics of the Equal-Spacing Array, $D_1/D_2 = 1.95$ (Slug - loaded). $l_s = 0.53\ D_1$.

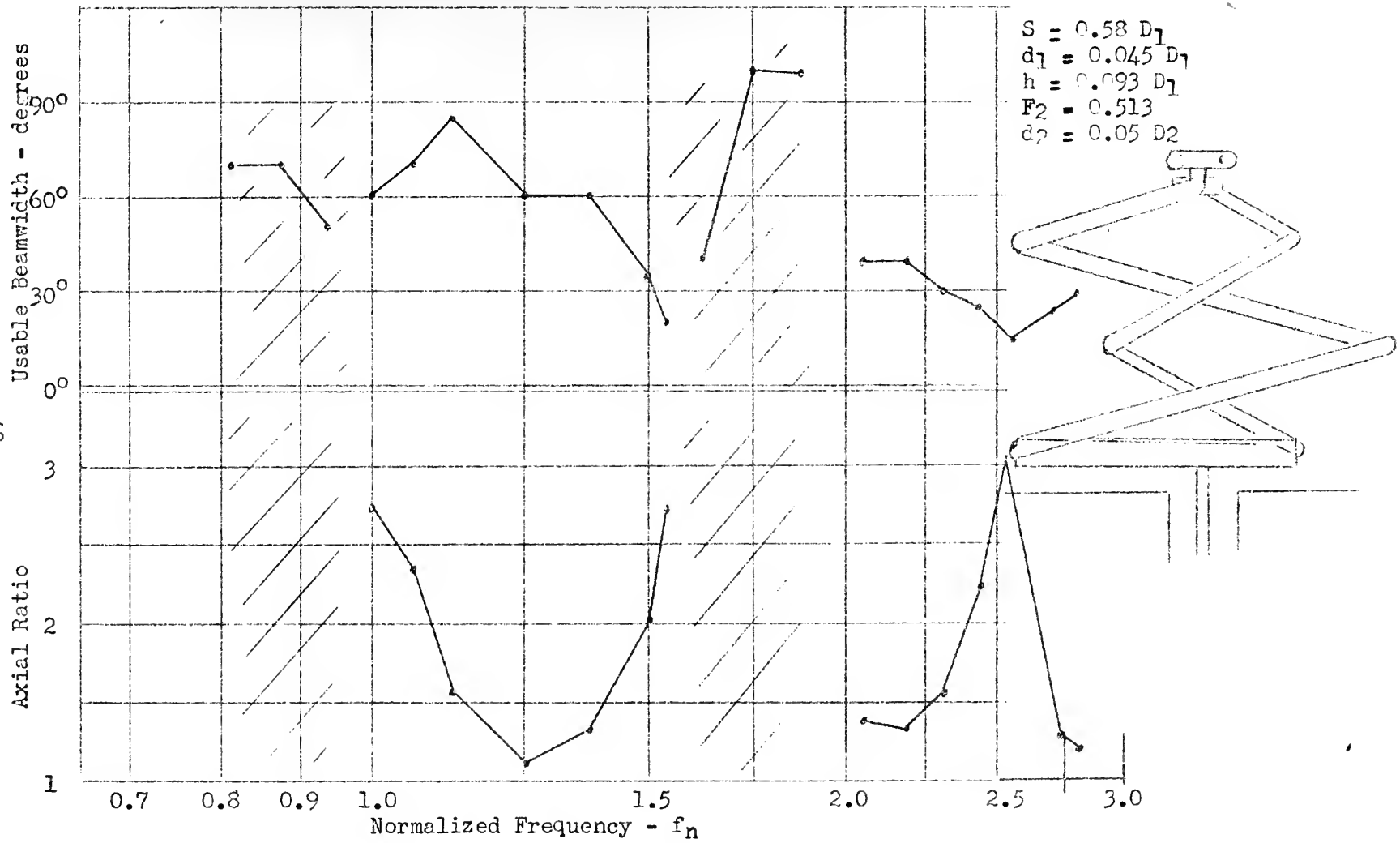

Fig. 16. Measured Radiation Pattern Characteristics of the Equal-Spacing Array, $D_1/D_2 = 1.95$.

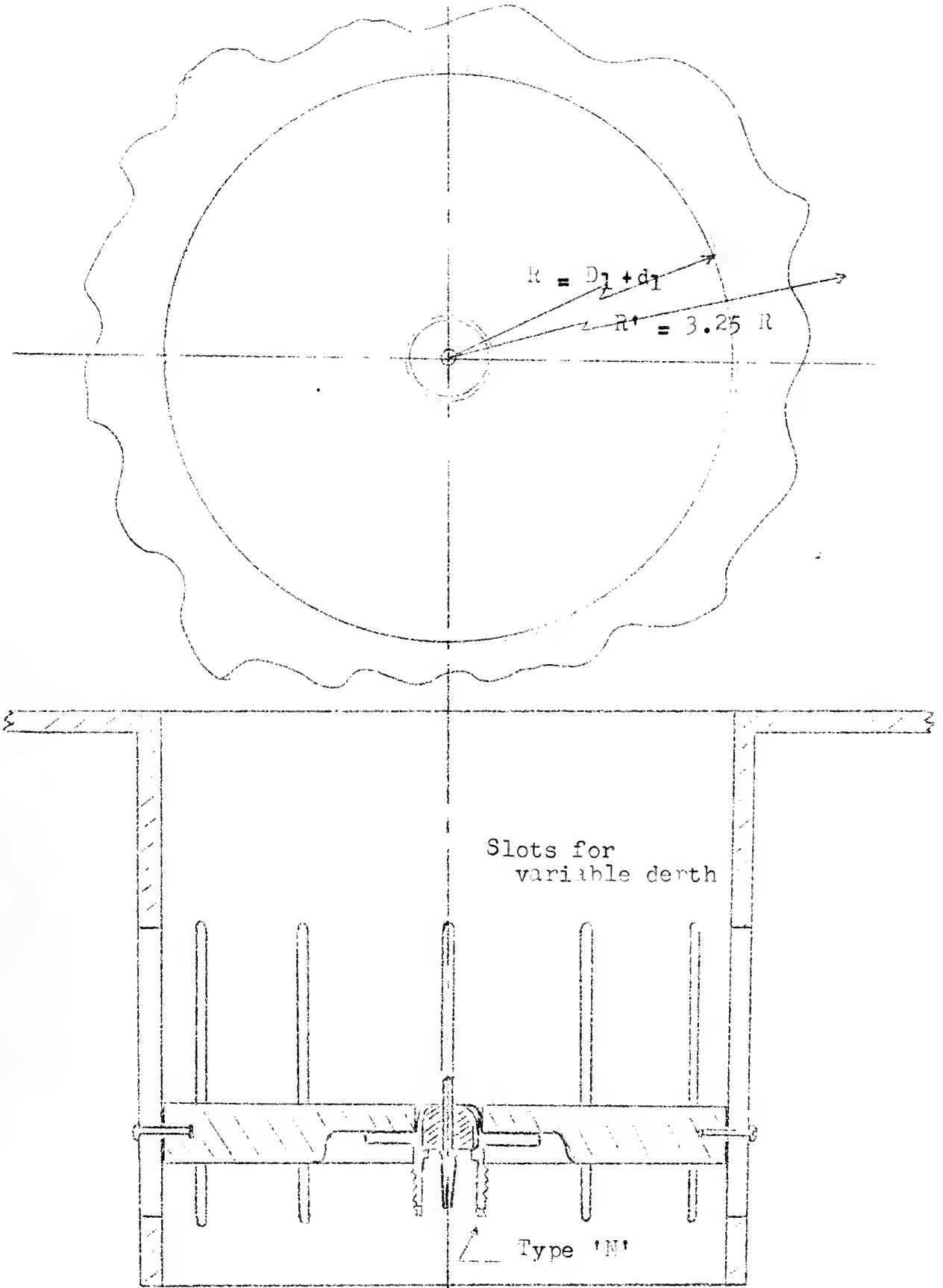

Fig. 18. The Cavity Mounting.

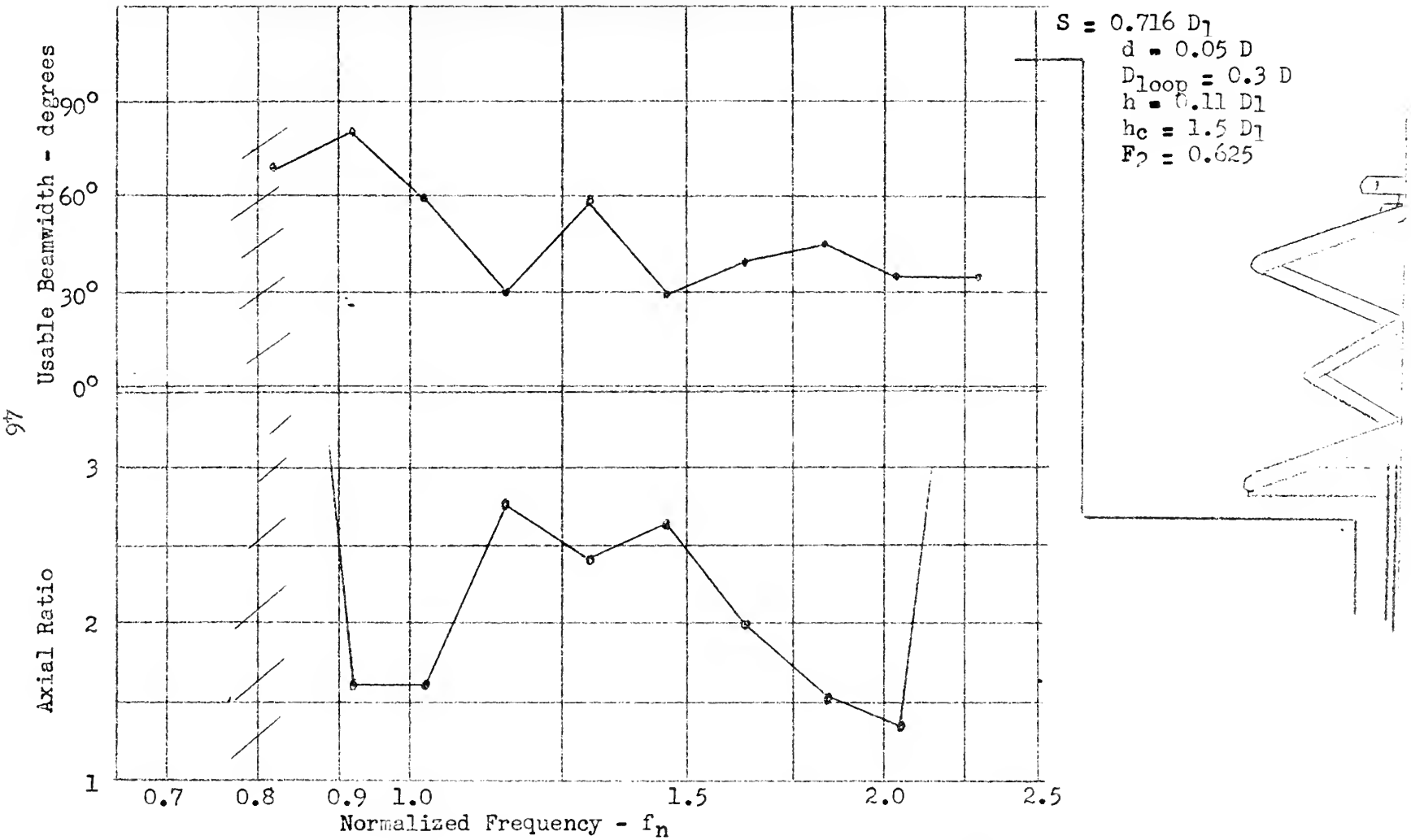

Fig. 19. Measured Radiation Pattern Characteristics of a Cavity-Mounted Array.

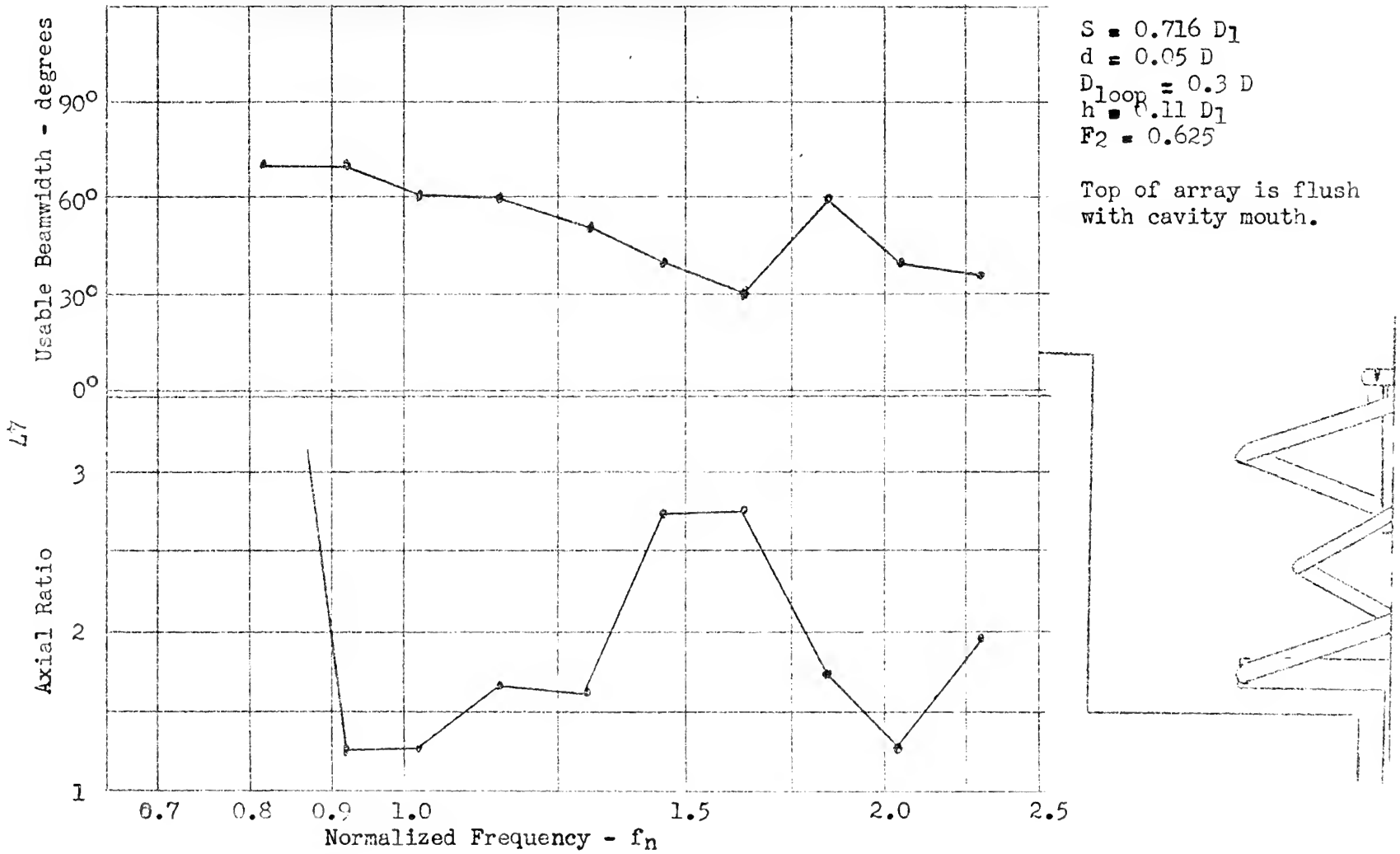

Fig. 20. Measured Radiation Pattern Characteristics of a Cavity-Mounted Array (Slug-loaded). l_s = 0.39 D_1.

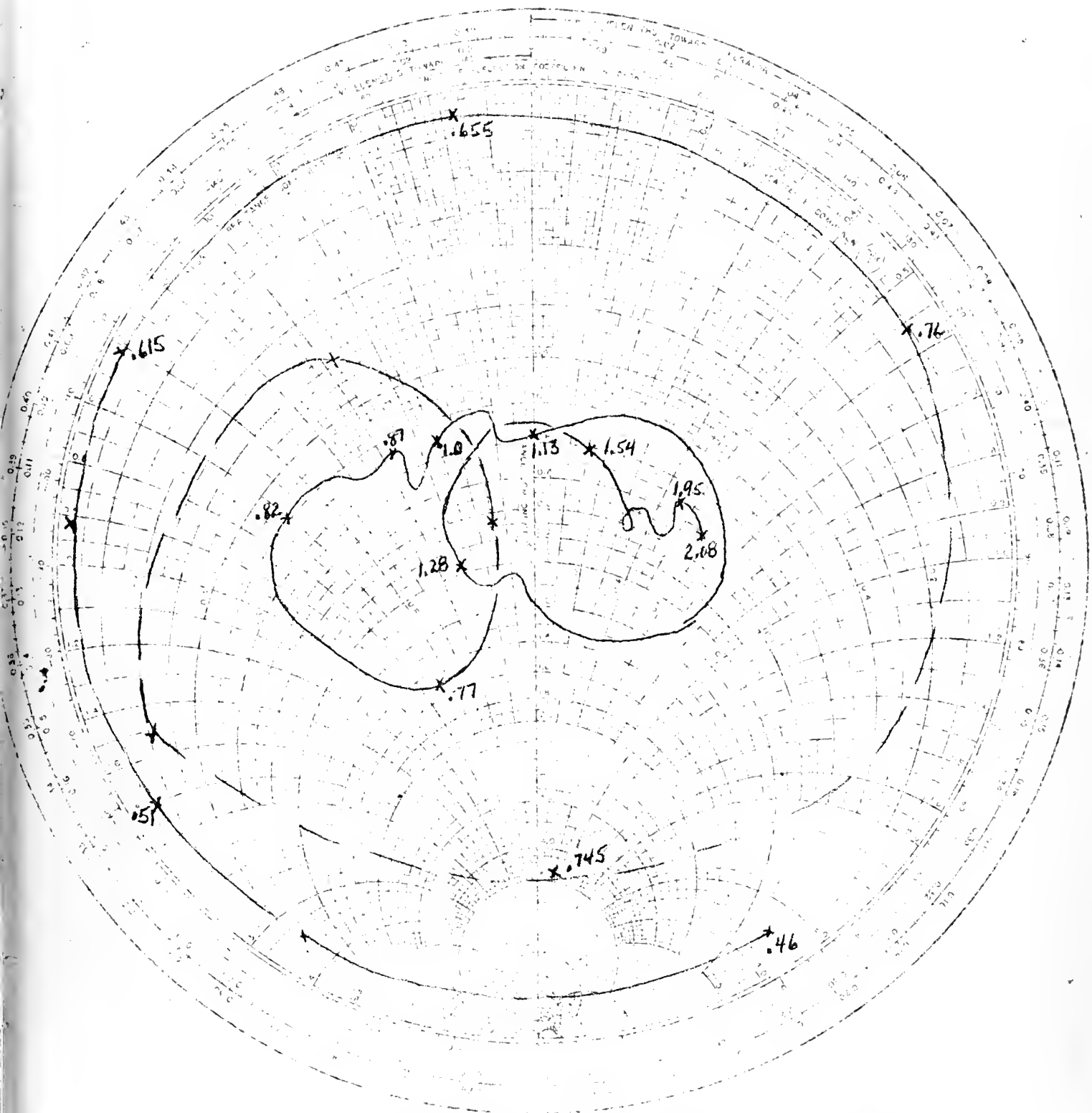

Fig. 21. Measured Impedance of a Cavity-Mounted Array. (Slug-loaded). Z_0 = 50 ohms. Normalized Frequencies.

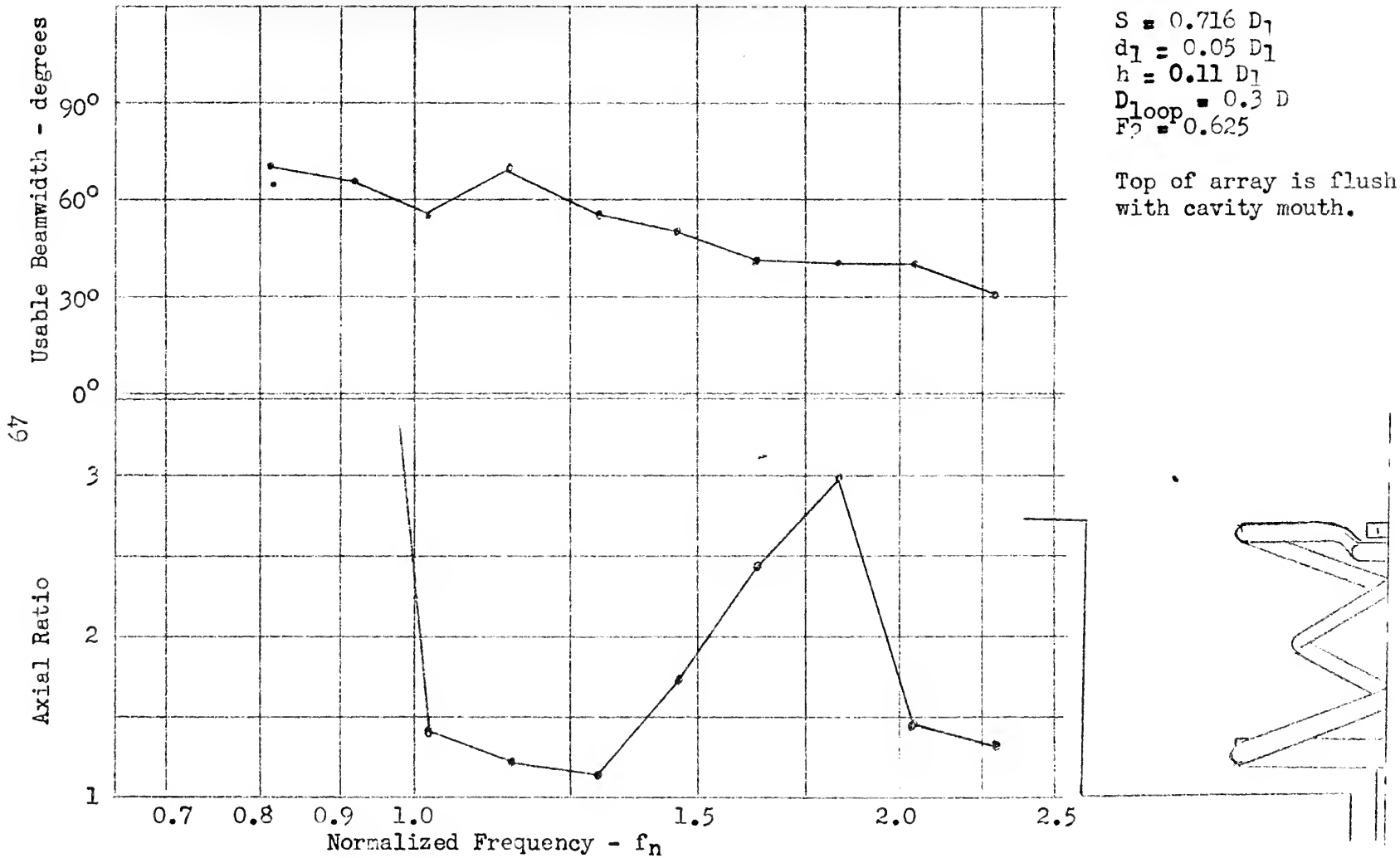

Fig. 22. Measured Radiation Pattern Characteristics of a 1-turn, Cavity-Mounted Array.

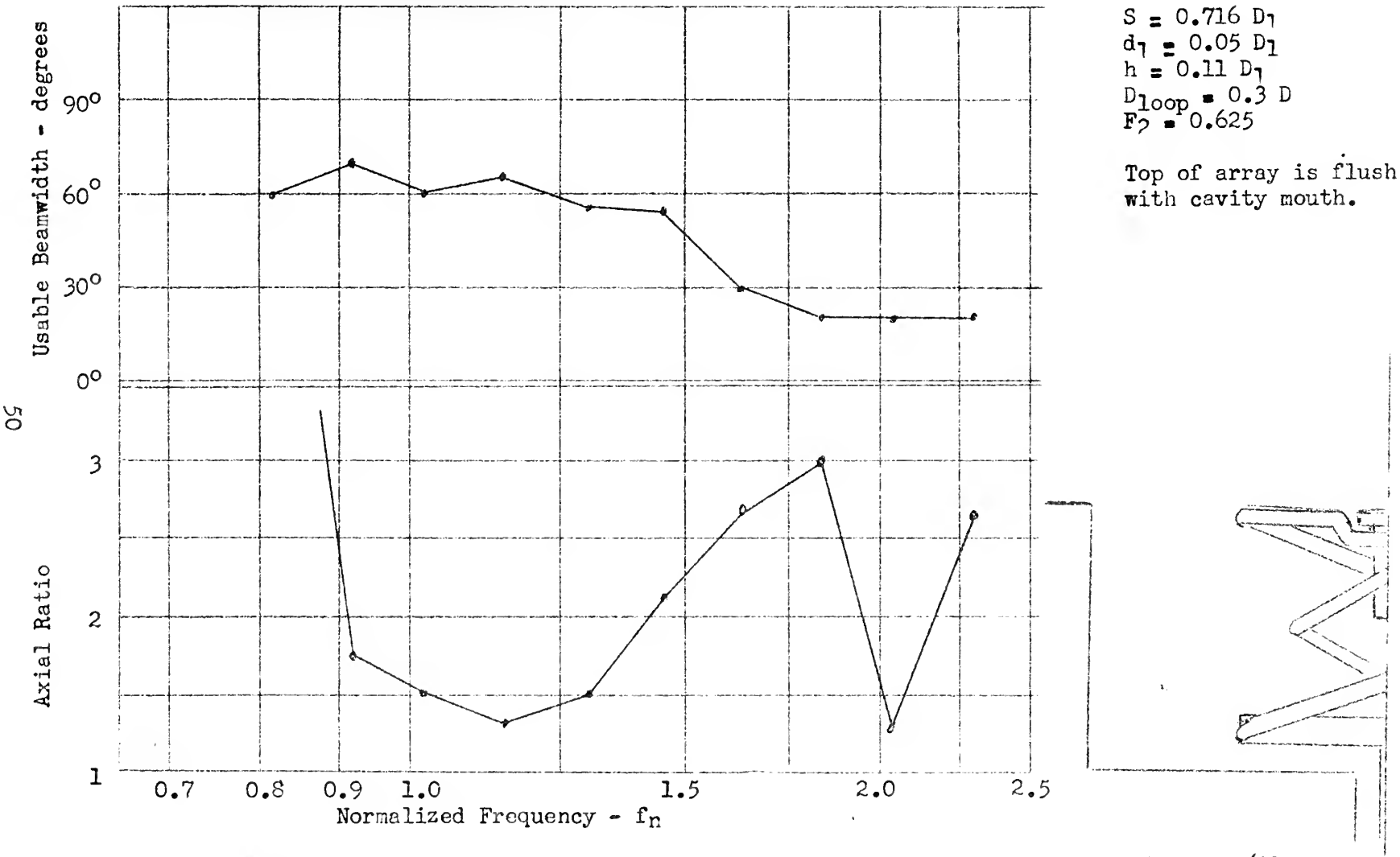

Fig. 23. Measured Radiation Pattern Characteristics of a 1-turn, Cavity Mounted Array (Slug-loaded). l_s = 0.39 D_1.

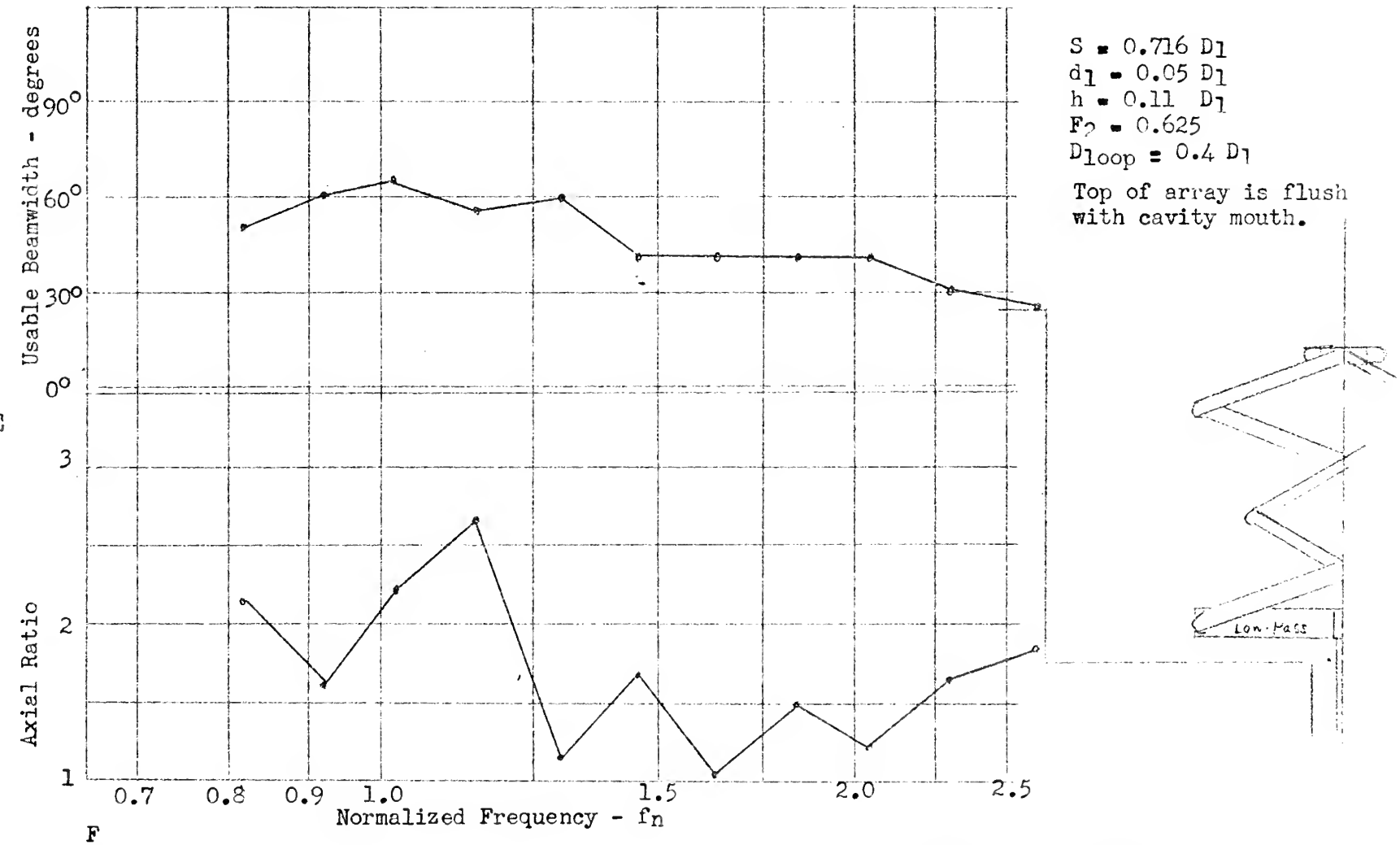

Fig. 24. Measured Radiation Pattern Characteristics of a Cross-Wound, Cavity-Mounted Array.

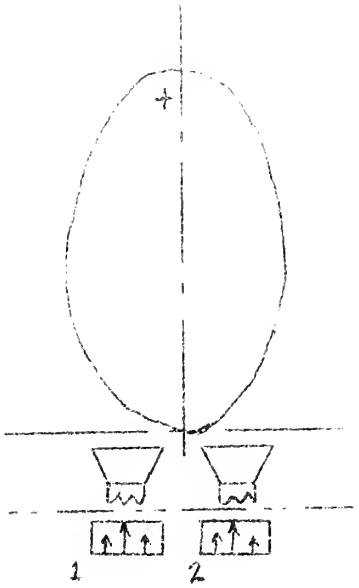

a. Radiation Pattern and Aperture Distributions for the even mode.

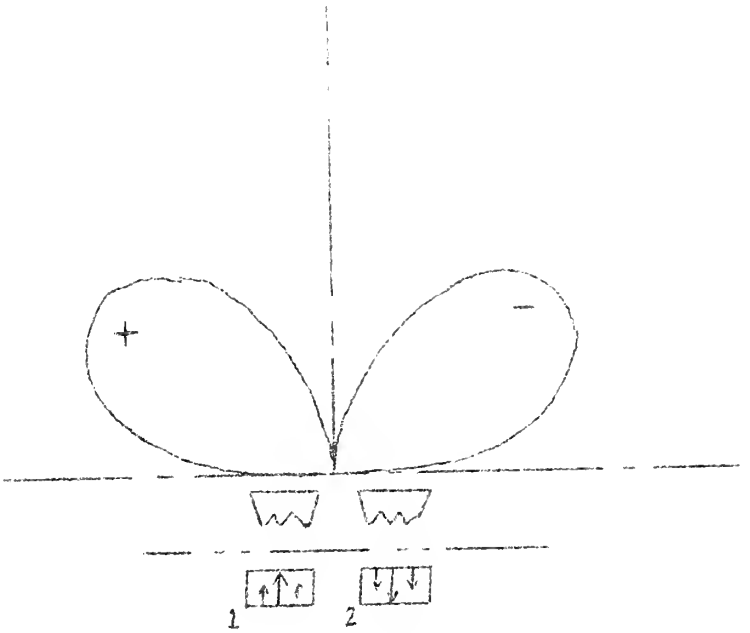

b. Radiation Pattern and Aperture Distributions for the odd mode.

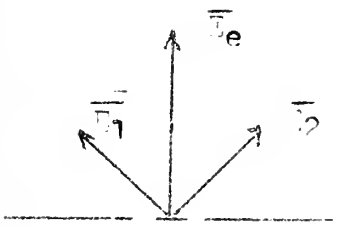

c. Phasor Representation of the Even Mode.

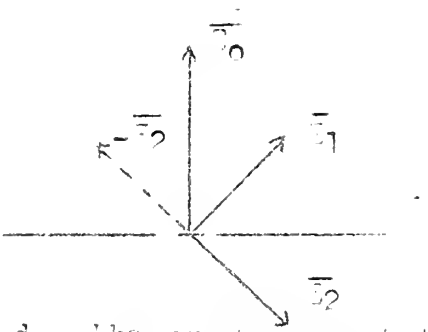

d. Phasor Representation of the Odd Mode.

Fig. 25. The Even and Odd Radiation Modes.

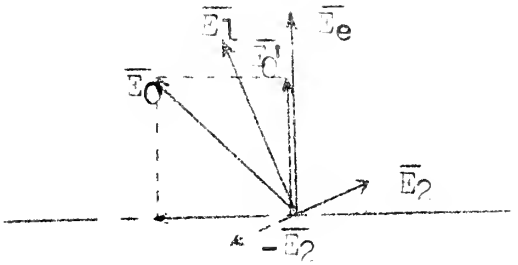

a. Phasor Representation of Multimoding Array where $|E_1| \neq |E_2|$.

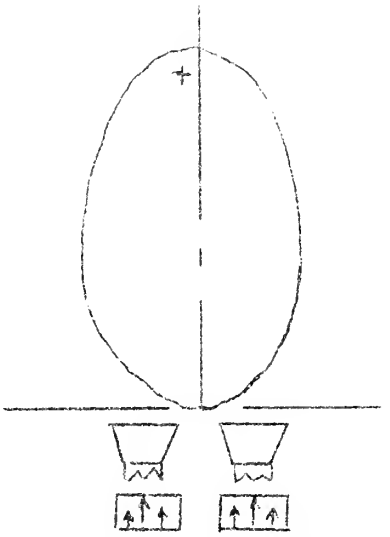

b. Instantaneous even mode Radiation Field.

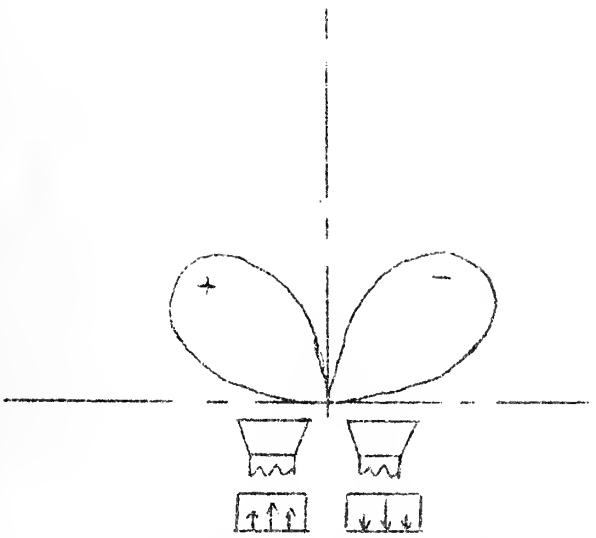

c. Instantaneous odd mode Radiation Field.

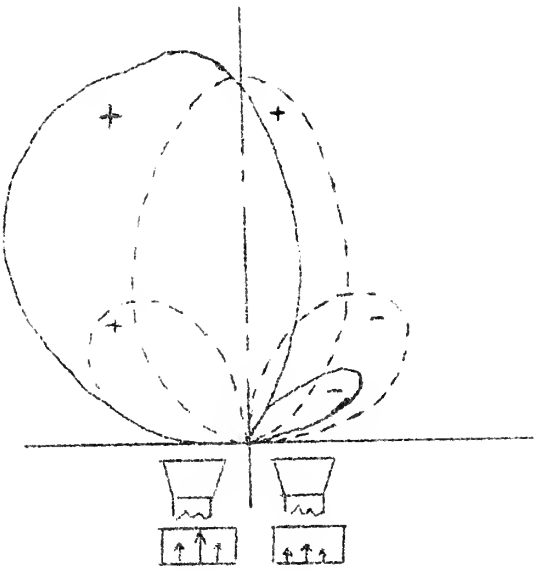

d. Instantaneous Radiation Field.

Fig. 26. Tilt of an Axial Beam Pattern due to Multimoding.

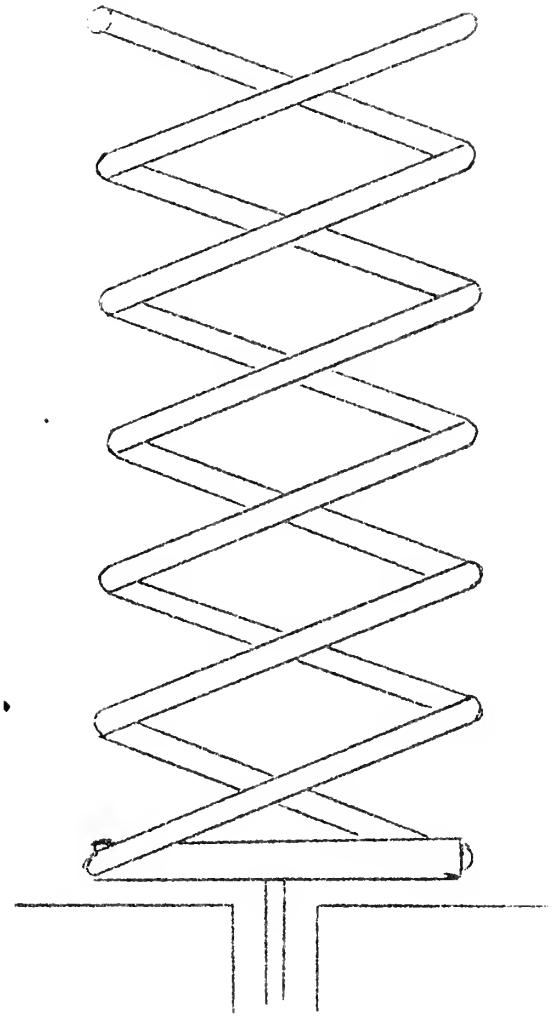

Fig. 27. The Concentric, "Odd-Mode" Array.

BIBLIOGRAPHY

1. S. A. Schelkunoff, Electromagnetic Waves, D. Van Nostrand Company, Inc., 1943.

2. J. D. Kraus, Antennas, McGraw-Hill Book Company, Inc., 1950.

3. J. D. Kraus, Helical Beam Antenna, Electronics, 20, pp. 109-111, April, 1947.

4. J. D. Kraus and J. C. Williamson, Characteristics of Helical Antennas Radiating in the Axial Mode, J. Appl. Phys., 19, pp. 87-96, January, 1948.

5. O. J. Glasser and J. D. Kraus, Measured Impedances of Helical Beam Antennas, J. Appl. Phys., 19, pp. 193-197, February, 1948.

6. J. D. Kraus, Helical Beam Antennas for Wide-band Applications, Proc. I.R.E., 36, pp. 1236-1242, October, 1948.

7. J. D. Kraus, The Helical Antenna, Proc. I.R.E., 37, pp. 263-272, March, 1949.

8. J. D. Kraus, Helical Beam Antenna Design Techniques, Communications, 29, pp. 6-9, 34-35, September, 1949.

9. T. E. Tice and J. D. Kraus, The Influence of Conductor Size on the Properties of Helical Beam Antennas, Proc. I.R.E., 37, p. 1296, November, 1949.

10. H. A. Wheeler, A. Helical Antenna for Circular Polarization, Proc. I.R.E., 35, pp. 1484-1488, December, 1947. This contains material of his oral presentation, Helical Antenna for Circular Polarization, given at the I.R.E. convention at New York, N.Y. in March, 1947.

11. E. T. Kornhauser, Radiation Field of Helical Antennas with Sinusoidal Current, J. Appl. Phys., 22, pp. 887-891, July, 1951.

12. W. Sollfrey, Wave Propagation on Helical Wires, J. Appl. Phys., 22, pp. 905-910, July, 1951.

13. H. L. Knudsen, Radiation Field of a Square, Helical Beam Antenna, J. Appl. Phys., 23, pp. 483-491, April, 1952.

14. J. S. Chatterjee, Radiation Field of a Conical Helix, J. Appl. Phys., 24, pp. 550-559, May, 1953.

15. M. Chodorow and E. L. Chu, Cross-Wound Twin Helices for Traveling-Wave Tubes, J. Appl. Phys., 26, pp. 33-43, January, 1955.

16. J. S. Chatterjee, Radiation Characteristics of a Conical Helix of Low Pitch Angle, J. Appl. Phys., 26, pp. 331-335.

17. P. Ferrer and E. S. Akely, Scattering of Electromagnetic Radiation by a Thin Circular Ring, J. Appl. Phys., 19, pp. 39-46, January, 1948.

18. A. Bystrom, Jr. and D. G. Berntsen, An Experimental Investigation of Cavity-Mounted Helical Antennas, I.R.E. Transactions on Antennas and Propagation, AP-4, pp. 53-58, January,1956.

19. P. W. Springer, End Loaded and Expanding Helices as Broad Band Circularly Polarized Radiators, Proc. Natl. Electronics Conf., Vol. 5, pp. 161-171, 1949.

20. O. C. Haycock and J. S. Ajioka, Radiation Characteristics of Helical Antennas of Few Turns., Proc. I.R.E., 40, pp. 989-991, August, 1952.

21. J. J. Dougherty, The Calculation, Measurement, and Maximumization of Radiation Efficiency of Loaded and Helical Short Antennas at Frequencies below Thirty Megacycles, Thesis, U. S. Naval Postgraduate School, 1953.

22. S. Ramo and J. R. Whinnery, Fields and Waves in Modern Radio, 2nd Ed., John Wiley and Sons, Inc., Chapman and Hall, Ltd., 1953.

23. I. M. Vann, Jr., A Review of Practices and Techniques for Broad-Banding Antennas, Thesis, U. S. Naval Postgraduate School, 1951.

24. E. C. Jordan, Electromagnetic Waves and Radiating Systems, Prentice-Hall, Inc., 1950.

25. V. J. Fowler, Analysis of Helical Transmission Lines by Means of the Complete Circuit Equations, I.R.E. Transactions on Antennas and Propagation, AP-2, October, 1954.

26. T. Crowley, Relations Between Impedance and Polarization, Project Report 339-21, Ohio State University Research Foundation, November, 1951.

Thesis
G252 Gates
Experimental study of concentric short helical antennas.